

LIQUID

DE83004755
SERI/STR-231-1812

September 1982

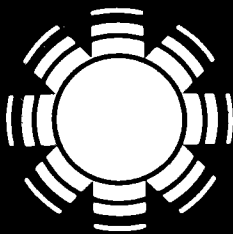
High Temperature Integrated Thermal Energy Storage System for Solar Thermal Applications

Final Subcontract Report

A. P. Bruckner
A. Hertzberg

Aerospace and Energetics Research Program
University of Washington
Seattle, Washington

Prepared Under Subcontract No. XP-0-9371-1



SERI

Solar Energy Research Institute

A Division of Midwest Research Institute

1617 Cole Boulevard
Golden, Colorado 80401

Operated for the
U.S. Department of Energy
under Contract No. EG-77-C-01-4042

Cat No: 23-7504

Printed in the United States of America
Available from:
National Technical Information Service
U.S. Department of Commerce
5285 Port Royal Road
Springfield, VA 22161
Price:
Microfiche \$3.00
Printed Copy \$6.50

NOTICE

This report was prepared as an account of work sponsored by the United States Government. Neither the United States nor the United States Department of Energy, nor any of their employees, nor any of their contractors, subcontractors, or their employees, makes any warranty, express or implied, or assumes any legal liability or responsibility for the accuracy, completeness or usefulness of any information, apparatus, product or process disclosed, or represents that its use would not infringe privately owned rights.

SERI/STR-231-1812
UC Category: 62

**High Temperature
Integrated Thermal Energy
Storage System for
Solar Thermal Applications**
Final Subcontract Report

A. P. Bruckner
A. Hertzberg

Aerospace and Energetics Research Program
University of Washington
Seattle, Washington

December 1982

Prepared Under Subcontract No. XP-0-9371-1

SERI Technical Monitor: Werner Luft

Solar Energy Research Institute

A Division of Midwest Research Institute

1617 Cole Boulevard
Golden, Colorado 80401

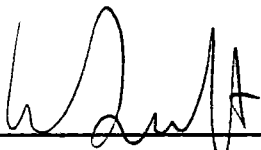
Prepared for the
U.S. Department of Energy
Contract No. EG-77-C-01-4042

FOREWORD

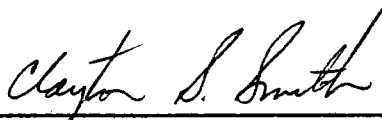
This report describes the results of work done by the University of Washington under subcontract XP-0-9371-1 to the Solar Energy Research Institute, as a part of task 1298, in WPA 348-82, in the Energy Storage Program. The work was performed over the period 04/15/81 to 09/14/82. The technical review of this work was done by John Wright and Robert Copeland.

Funds for this work were provided by the Division of Energy Storage Technology of the U. S. Department of Energy.

Approved for the
SOLAR ENERGY RESEARCH INSTITUTE



Werner Luft, Manager
Solar Energy Storage Program



Clayton S. Smith, Manager
Solar Fuels and Chemicals Research Division

EXECUTIVE SUMMARY

This report covers analysis, conceptual design, and experimental work for very high temperature (1400 °C) thermal energy storage. Anticipated applications are 1) fuels and chemicals production 2) process heat, and 3) electric power. This study was conducted for a 23MW_t (or 10 MW_e) solar energy system encompassing a solar thermal central receiver and a Brayton-cycle electric generator.

The heat transfer and storage medium is a glassy slag. Beads of slag are melted by direct-contact heat exchange in the solar central receiver. The molten slag is stored at 1650 K in an insulated storage vessel. Sensible heat is extracted from the molten slag in a direct-contact heat exchanger in which the slag is sprayed through a high-pressure counter flowing working gas. The 1500 K hot gas operates a 43% efficiency regenerative Brayton gas turbine. The solidified slag droplets at 985 K are returned to the central receiver to repeat the cycle.

The objective is to demonstrate the technical and economic feasibility of this system concept.

The scope of the work included (1) an investigation of the thermophysical and chemical properties of candidate thermal energy storage media and containment vessel materials, (2) analysis of heating and melting of the storage medium in the solar central receiver, (3) study of storage medium handling and transport including design of slag pump and bead transport system, (4) development of droplet heat exchanger model, (5) design of the thermal storage subsystem, and (6) determination of capital, operating, and maintenance costs using a prescribed methodology and specific economic parameters.

Slag selection was made on the basis of: low (< 1 Pa-s) viscosity at the melting point, melting point around 1600 K, relatively high surface tension, low vapor pressure, stability at high temperature, and high heat capacity.

The selected material, 50% SiO₂, 30% CaO, and 20% MgO, has a liquidus temperature of 1630 K, a viscosity of 0.51 Pa-s (5.1 poise) at 1673 K, density of 2.9 g/cm³, surface tension of 0.42 N/m (420 dyne/cm) at 1673 K, specific heat of 1.22 kJ/kg-K (0.292 cal/g C), and a partial pressure for SiO at 1650 K of 3.5 mPa (3.45 x 10⁻⁸ atm).

The selected insulation for the storage tank is fused-cast alpha-alumina (99.3% Al_2O_3) having high resistance to basic slags. The corrosion rate at the melt line at 1650 K is about 0.2 mm per day, giving a 6-year life for 45 cm thick insulation.

The 10 slag pumps are also lined with fused-cast alpha-alumina and use sliding valves and air pressure a 25 atm to move the slag from the storage tank to the direct-contact heat exchanger.

The droplet heat exchanger (6.5 m high and 3 m in diameter) is lined with graphite blocks. Pressurized slag is injected via a molybdenum injector plate and forms 1 mm droplets that solidify before hitting the bottom of the heat exchanger at 980 K. The baseline design uses 20 atm argon as the working gas. The net loss of argon through pressure locks at the bottom of the heat exchanger is 0.67 kg/h

An the economic analysis was performed. The costliest items, either energy or power related, are 1) the fused-cast alpha-alumina liners for tanks, pumps, and pipes, 2) the slag pumps, and 3) the droplet heat exchanger. The capital investment costs range from \$226/kWh for one hour storage capacity to \$18/kWh for 48 hours of storage capacity.

Conclusions

- a. Experiments with molten slag droplet formation was performed. Although the experiments encountered difficulties, droplet formation (in the range of 1 to 3 mm of diameter) was achieved.
- b. A conceptual design of molten-salt thermal storage subsystem was generated together with applicable cost data.
- c. By comparison with other thermal storage technologies for electric power production, molten slag is more costly at all storage capacities.
- d. The major cost elements are the storage tank insulation, slag pumps, and heat exchanger.
- e. The cost of the molten slag is very low in comparison with other storage media.

Recommendations

The slag is low cost, but cost reductions are needed in capital (energy related) costs and power related costs. The following research activities are recommended to improve the potential of this technology:

- a. Search for lower-cost insulation techniques.
- b. Search for lower cost slag pumping.
- c. Generate a conceptual design for a lower-cost subsystem and evaluate the costs.
- d. Perform additional experiments to provide quantitative data on droplet formation.
- e. Perform experiments that measure the heat transfer rate with multiple droplets.

Werner Luft, Manager
Solar Energy Storage Program
SOLAR ENERGY RESEARCH INSTITUTE

TABLE OF CONTENTS

| | <u>Page</u> |
|---|-------------|
| 1.0 INTRODUCTION | 1 |
| 1.1 Background | 1 |
| 1.2 Objectives | 5 |
| 2.0 CANDIDATE STORAGE MATERIALS | 6 |
| 2.1 Overview | 6 |
| 2.2 Viscosity | 7 |
| 2.3 Surface Tension | 10 |
| 2.4 Heat Capacity | 11 |
| 2.5 Thermal Conductivity | 14 |
| 2.6 Vapor Pressure | 14 |
| 3.0 THE ENERGY STORAGE SYSTEM | 19 |
| 3.1 Overview | 19 |
| 3.2 General Considerations | 19 |
| 3.3 Molten Slag Storage Tank | 23 |
| 3.4 Storage Tank Feed Pipe | 31 |
| 3.5 Emergency Slag Dump | 31 |
| 3.6 Molten Slag Pumps | 32 |
| 3.7 Droplet Heat Exchanger | 34 |
| 3.8 Temporary Slag Storage Bin | 37 |
| 3.9 Vertical Bucket Conveyor | 38 |
| 3.10 Solar Central Receiver | 38 |
| 4.0 ECONOMIC ANALYSIS | 42 |
| 4.1 Methodology | 42 |
| 4.2 Component Capital Costs | 44 |
| 5.0 CONCLUSIONS AND RECOMMENDATIONS | 53 |
| 5.1 Conclusions | 53 |
| 5.2 Recommendations | 54 |
| 6.0 REFERENCES | 56 |
| APPENDIX A: Small-Scale Experiments with Molten Slags | 60 |
| APPENDIX B: Droplet Generation | 68 |
| APPENDIX C: The Droplet Heat Exchanger | 75 |
| APPENDIX D: Contamination of the Working Gas by Slag Vapor | 91 |
| APPENDIX E: Injection and Transport Losses | 94 |
| APPENDIX F: Working Gas Losses | 96 |
| APPENDIX G: Radiative Heating of Slag Beads in Solar Receiver | 98 |

LIST OF FIGURES

| <u>Figure</u> | <u>Page</u> |
|--|-------------|
| 1. High temperature 10 MW _e solar thermal power plant using molten slag thermal energy storage and direct contact heat exchange | 3 |
| 2. Variation of viscosity with temperature and composition of molten CaO-MgO-Al ₂ O ₃ -SiO ₂ slags | 8 |
| 3. Thermal conductivity of fused silica | 15 |
| 4. Calculated vapor pressures of principal decomposition products of silica in a neutral atmosphere | 18 |
| 5. Schematic of slag thermal energy storage system | 20 |
| 6. Cross-section of molten slag storage tank | 26 |
| 7. Cross-sectional view of reciprocating molten slag pump and inlet and exit pipes | 33 |
| 8. Schematic of high temperature droplet heat exchanger | 35 |
| 9. Schematic of conceptual design of solar receiver for melting slag beads | 39 |
| A-1. Schematic of experimental apparatus for molten slag droplet generation | 64 |
| B-1. Geometry of jet breakup | 70 |
| C-1. Schematic of 1-D droplet heat exchanger model | 77 |
| C-2. Axial velocity profiles in droplet heat exchanger for heating argon at 20 atm. Droplet dia = 1 mm | 85 |
| C-3. Axial temperature profiles in droplet heat exchanger for heating argon at 20 atm. Droplet dia = 1 mm. Optically thick approximation | 87 |
| C-4. Axial temperature profiles in droplet heat exchanger for heating argon at 20 atm. Droplet dia = 1 mm. Optically thin approximation; emissivity of droplet = 0.5. Adiabatic blackbody side wall temperature computed by Hottel's zone method | 88 |
| F-1. Rotary valve depressurizer | 97 |
| G-1. Axial temperature profiles of slag beads falling at terminal velocity through vertical cylindrical solar receiver cavity for various solar fluxes | 101 |

LIST OF TABLES

| <u>Table</u> | <u>Page</u> |
|---|-------------|
| 1. Slags Investigated Experimentally | 9 |
| 2. Surface Tension Factors | 10 |
| 3. Slag and Gas Flow Conditions for 23 MW(th), 10 MW(e) Plant | 22 |
| 4. Wall and Floor Insulation Parameters | 28 |
| 5. Roof Insulation Parameters | 28 |
| 6. Formulae Used in Cost Analysis | 43 |
| 7. Material Unit Costs | 45 |
| 8. Storage Tank Costs | 46 |
| 9. Power-Related Costs | 46 |
| 10. Component Costs for High Temperature Slag Thermal Energy Storage System | 47 |
| 11. Cost Calculations (in 1000\$) for 23 MW(th) Slag Storage System | 48 |
| 12. Thermal Storage Economic Evaluation for the High Temperature Slag Storage System | 50 |
| A-1. Compositions of the Raw Materials Used for Slag Manufacture | 61 |
| A-2. Slag Compositions and Batch Formulas (Weight Percent) | 62 |

1.0 INTRODUCTION

1.1 Background

An efficient and economical energy storage system must be an integral part of all solar central generating plants due to the intermittent nature of the solar energy resource. In recent years a variety of thermal energy storage concepts have been investigated.^{1,2} Typically, thermal energy is stored in a suitable medium either as sensible heat or latent heat, or both. Examples are organic fluid/rock, air/rock, liquid metal, and molten salt storage systems. Existing storage concepts all operate at temperatures below about 1100°K due to the materials limitations imposed by heat exchange apparatus of conventional tube and shell design. Thus, the availability of the thermodynamic potential of solar radiation is severely degraded prior to its use in a heat engine or chemical processing plant.

High efficiency in a thermal system invariably leads to high temperature. Hertzberg has identified a number of promising power generation cycles with efficiencies from 45% to 70%, involving peak temperatures of up to 2000°K.³ To capitalize on the high efficiency potential of such cycles, high temperature heat storage facilities and heat transfer devices are required for central solar energy stations based on these cycles. A similar argument is applicable to the use of solar central systems for chemical processing. High-temperature process heat and thermochemical fuels and chemicals production would offer favorable thermodynamics if carried out at temperatures above the capability of current heat exchanger and thermal storage technologies.⁴

Capacitive heat exchangers and storage systems circumvent tube wall temperature limitations by using high temperature materials and transporting them into direct contact with the heat source. Common examples are packed bed regenerative heat exchangers and fluidized bed heat exchangers.⁵ Solid phase capacitive elements, which must operate in a cyclic fashion, are subject to physical degradation due to thermal shock and represent a high fraction of the total system cost involved. The problems of these systems become increasingly acute as the maximum temperature and rate of temperature change are increased.

The approach described in this report is based on the premise that the classical inefficiencies associated with capacitive heat exchangers can be circumvented if the capacitive elements are mobile and are remanufactured during each temperature cycle, eliminating the degradation due to thermal shock. Specifically, the concept involves the phase conversion of a glassy, siliceous slag, which is very stable at high temperatures, to a liquid in a solar-central receiver and the extraction of sensible heat from the slag in a direct contact droplet heat exchanger. This material is a very inexpensive substance, widely available and benign in its contact with the environment. Thermal energy storage equipment is an integral part of the system. Storage temperature can be high enough to make use of the maximum thermodynamic potential of solar radiation, even allowing for reradiation losses.

A schematic of a proposed 10 MW_e solar thermal power plant which utilizes the novel heat exchanger and storage system appears in Fig. 1. The working material is delivered to the top of the solar receiver tower as a uniform aggregate of small beads, which are melted by a combination of direct solar radiation and reradiation from the cavity walls. The resulting

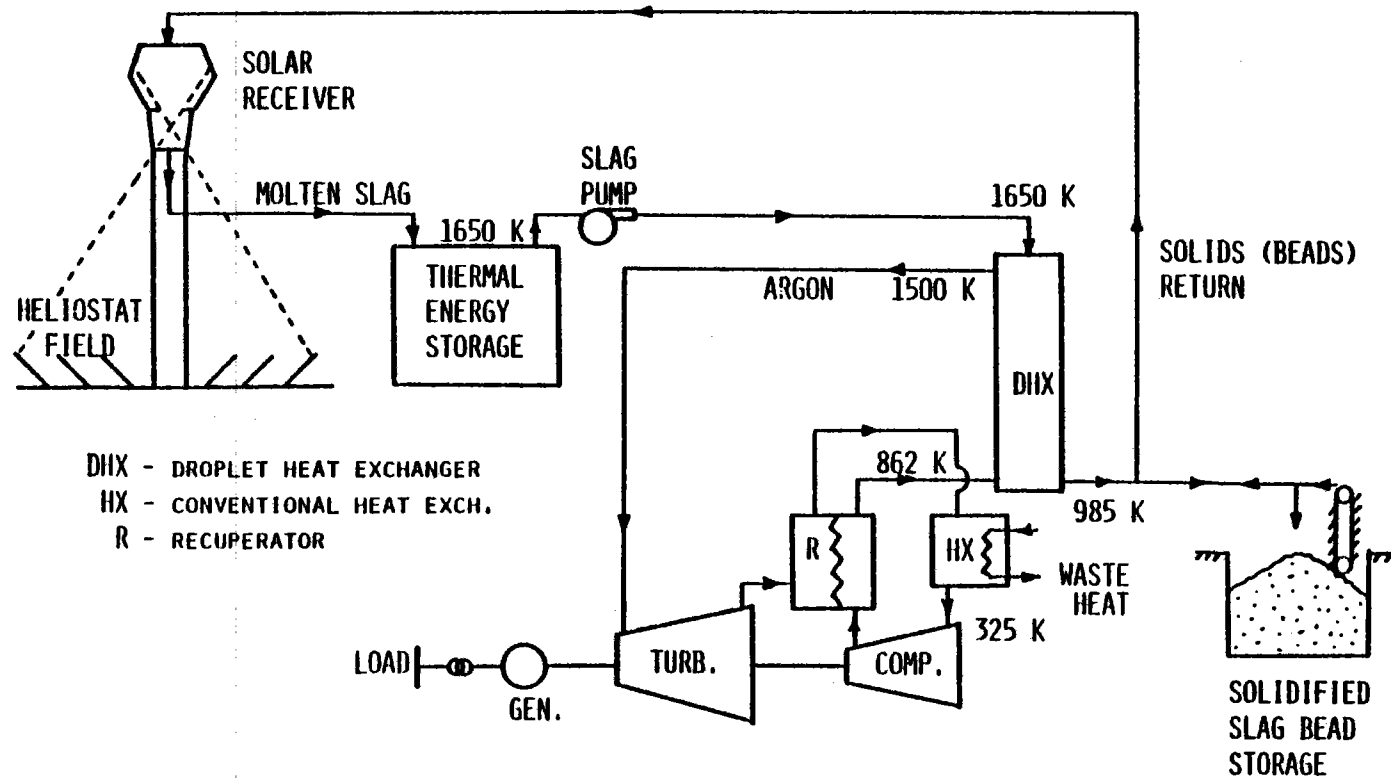


Fig. 1 High temperature 10 MW_e solar thermal power plant using molten slag thermal energy storage and direct contact heat exchange.

liquid collects in a crucible at the bottom of the receiver and flows down a refractory conduit to the thermal storage vessel and thence to the direct-contact heat exchanger. The molten material is injected into the heat exchanger under pressure as a large number of small diameter streams, which break up into droplets. The droplets fall through a counterflowing high pressure working gas, giving up their heat by convection, conduction and radiation and changing phase into the solid bead state in the process. The solidified beads are collected at the bottom of the heat exchanger as an aggregate and delivered directly back to the solar receiver or to a temporary solids storage bin. The heated gas is removed at the top of the heat exchanger and employed by a regenerative Brayton cycle at a temperature range corresponding to the necessary operational parameters of the system desired.

A unique feature of this system is that thermal storage is accomplished at the same high thermodynamic potential at which the solar radiation is absorbed in the solar collector. The high efficiency at which the energy conversion and storage take place reflects favorably back through the cost of the entire solar energy system. More useful energy is obtained from a smaller heliostat field and other components.

Although the molten slag solar thermal concept outlined above has a variety of other promising applications, such as chemical processing, the scope of this report is limited to the study of its application to electric power generation. Performance and cost data are presented for the 10 MW_e baseline design shown in Fig. 1 for 1, 6, 15 and 48 hour thermal storage.*

*The economic analysis was carried out by R. Taussig, Mathematical Sciences Northwest, Inc., Bellevue, WA, under a subcontract.

1.2 Objectives

The objectives of this study are to:

- 1) Investigate the thermophysical and chemical properties of potential glass-like storage media and containment vessel materials.
- 2) Analyze the heating and melting of the storage material in the cavity solar receiver.
- 3) Study storage material handling and transport.
- 4) Develop an analytical model of the droplet heat exchanger.
- 5) Develop capital cost and present worth revenue requirement data from a 10 MW_e point design for 1, 6, 15 and 48 hour storage.

2.0 CANDIDATE STORAGE MATERIALS

2.1 Overview

The choice of a suitable thermal storage material for the proposed system is limited by considerations which are fairly unique to high temperature materials science. The material must have a melting point in the range desired for an operating and storage temperature and should also exhibit relatively low viscosity and high surface tension under the prescribed conditions to facilitate droplet formation in the droplet heat exchanger. Furthermore, the material should have low vapor pressure to avoid loss of material and contamination of the working gas in the droplet heat exchanger. Since the material is exposed to air in the solar receiver, it should be stable at high temperatures under oxidizing conditions. Also desirable are a high heat capacity and a high heat of fusion. Finally, the material should be very low in cost.

The selection of a pure substance limits the application temperature to the melting temperature of the substance. This limitation can be circumvented to some extent by selecting intermediate compositions between or among pure components. Current design proposes peak temperatures in the range of about $\sim 1650\text{-}1750^\circ\text{K}$ in the storage vessel and the heat exchanger. The material chosen must therefore have a melting point below this range.

Although salts exhibit low melting temperatures, high heat of fusion, and low viscosity, they suffer from high volatility⁶ and high cost,² and therefore are not suitable materials for our storage concept. Metal oxides, on the other hand, are inexpensive, have low volatilities and are stable under oxidizing conditions at high temperatures.⁷ The range of viscosities and surface tensions exhibited by metal oxides is also within the

requirements for droplet formation.⁸ Accordingly we have investigated the properties of metal oxides as candidate high temperature thermal storage materials. In what follows we discuss each of the critical properties in detail.

2.2 Viscosity

Materials with viscosities of 10 poise or less at their melting point are required in order to facilitate droplet formation in the heat exchanger. A number of pure metal oxides exhibit viscosities of under 1 poise in the vicinity of their melting temperatures and have other desirable properties.⁹ However, their melting points tend to be too high to be of interest. Common glass formers on the other hand, such as silicates, have low melting temperatures but exhibit complex "framework" structures in which every SiO_4 tetrahedron is coordinated with its neighbors.¹⁰ These melts require the addition of some form of network modifier to break up the cross-linking, thereby freeing the structure and bringing the viscosity down to a workable range. Modifiers such as alkali oxides and basic oxides can decrease viscosity values by many orders of magnitude.¹¹⁻¹⁷

The system $\text{SiO}_2\text{-CaO-MgO-Al}_2\text{O}_3$, which is similar to metallurgical slags, appears particularly attractive, not only from the point of view of low viscosity,¹⁴⁻¹⁷ but also because of the very low vapor pressure and high chemical stability of its components.⁷ Viscosities as low as 2 poise are possible at temperatures of interest.¹⁴

Turkdogan and Bills¹⁷ have reviewed the literature on the viscosity of $\text{CaO-MgO-Al}_2\text{O}_3\text{-SiO}_2$ melts and have published curves of the variation of viscosity with temperature and composition of these melts. Figure 2 reproduces one of the figures in their paper. The various curves represent different values of the sum of the mole fraction of SiO_2 and the silica

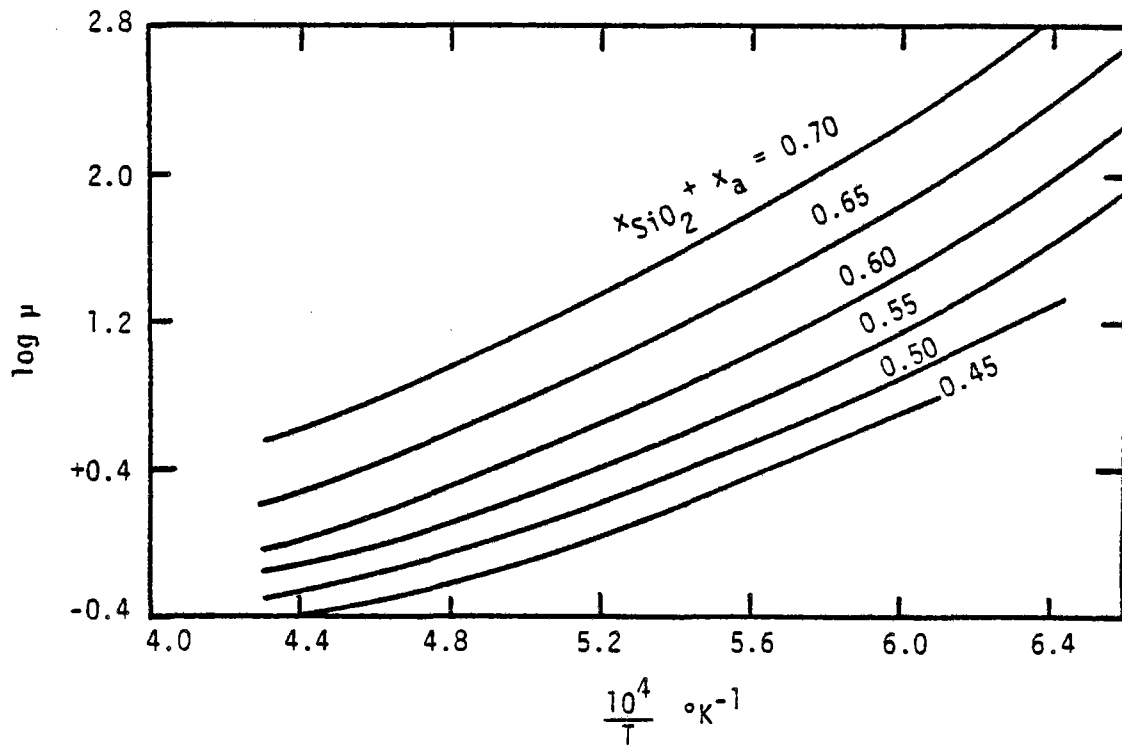


Fig. 2 Variation of viscosity with temperature and composition of molten CaO-MgO-Al₂O₃-SiO₂ slags. (x_{SiO_2} and x_a are the mole fraction of silica and the silica equivalence of alumina, respectively).¹⁷

equivalence of Al_2O_3 . Increasing the concentration of SiO_2 or Al_2O_3 increases the viscosity. Increasing the concentration of CaO or MgO decreases the viscosity. On a molar basis, CaO and MgO have the same effect on viscosity.

Two slag compositions of low melting temperature and low viscosity that we have studied experimentally (see Appendix A) are listed in Table 1.

TABLE 1
Slags Investigated Experimentally

| | <u>Composition by Weight</u> | | | | <u>Liquidus Temperature</u> ^{18,19} | <u>Viscosity (poise)</u> ^{14,15} | |
|--------|------------------------------|-----|-----|-----------|--|---|--------|
| | SiO_2 | CaO | MgO | Al_2O_3 | | 1723°K | 1673°K |
| Slag A | 40% | 35% | 20% | 5% | 1708°K | 2.64 | -- |
| Slag B | 50% | 30% | 20% | -- | 1630°K | 3.56 | 5.10 |

Slag A exhibits about 25% lower viscosity than Slag B but has a higher liquidus temperature^{18,19} (i.e., the temperature above which the mixture is all liquid), which increases the possibility of its solidifying in the storage vessel, slag conduits or heat exchanger injector if plant shut-down for significant time periods occurs. Accordingly, Slag B appears to be the most attractive droplet material at this time. Its viscosity varies from ~7 poise at 1650°K to ~2.5 poise at 1750°K, well within the range of acceptability. This slag corresponds to the lowermost curve in Fig. 2.

The density of Slag B in the molten state is 2.9 g/cm^3 , as calculated from the measured density of the solid, assuming a 10% increase in specific volume on melting.¹⁰

2.3 Surface Tension

The surface tension of a slag can be calculated by a method originally due to Dietzel.²⁰ He showed that the value of surface tension of a glass or slag at a given temperature can be represented as the sum of a series of values associated with the oxides in the mixture, where each oxide component value is obtained by multiplying the percentage weight of that oxide by a characteristic factor. These factors for the oxides of interest here are listed in Table 2 for a temperature of 1673°K.²¹ The surface tension of Slag B at this temperature is thus 420 dyne/cm. The temperature coefficient of surface tension is a function of composition but for mixtures of the components in Table 2 it is negative and of the order of 0.01-0.02 dyne/cm per °K.²¹

TABLE 2
Surface Tension Factors

| <u>Oxide</u> | <u>Surface Tension Factor²¹ (dyne/cm) for 1% oxide at 1673°K</u> |
|--------------------------------|---|
| SiO ₂ | 3.24 |
| CaO | 4.92 |
| MgO | 5.49 |
| Al ₂ O ₃ | 5.85 |

2.4 Heat Capacity

The total amount of heat which can be stored within a material and subsequently transferred to a working gas is given by:

$$\overline{\Delta H}_{\text{tot}}^{\circ} = \int_{T_1}^{T_2} \overline{C}_p dT + \overline{\Delta H}_F^{\circ} \quad (1)$$

where $\overline{\Delta H}_{\text{tot}}^{\circ}$ and $\overline{\Delta H}_F^{\circ}$ are the total enthalpy and heat of fusion per mole of material respectively, \overline{C}_p is the molar heat capacity at constant pressure and T_1 and T_2 represent the initial and final temperatures, respectively.

Since practical considerations relating to storage vessel construction (see Section 3.3) limit the size of the containment vessels, the critical property is not the heat transfer per mole of material, but rather the heat stored per unit volume of material. Equation 1 then becomes

$$(\overline{\Delta H}_{\text{tot}}^{\circ})/\text{VOLUME} = \frac{(\overline{\Delta H}_{\text{tot}}^{\circ})\rho}{M} \quad (2)$$

where ρ is the density and M is the molecular weight of the material.

One can readily see that a composition of high heat capacity, high heat of fusion, high liquid density, as well as a relatively low molecular weight, would increase the desired heat storage. The higher melting or more refractory constituents of the slag are those that have the greatest contribution to the heat storage.⁷ This observation should be kept in mind when considering alternative materials.

Utilizing the heat of fusion of a refractory oxide requires the strict following of specific thermodynamic rules. The melting point of a solid is defined as the temperature at which the free energy of the solid form is equivalent to that of the liquid form. (The free energy is often referred

to as Gibbs' free energy and is defined as follows: $\bar{G} = \bar{H} - T\bar{S}$, where \bar{G} , \bar{H} and \bar{S} are the molar free energy, molar enthalpy, and molar entropy, respectively, and T refers to the absolute temperature in degrees Kelvin.) Since there is no change in free energy associated with melting, the change in enthalpy, or total heat transfer, is given by the product of the absolute temperature and the entropy change, $T\Delta S_F^\circ$, where ΔS_F° refers to the standard entropy change of fusion. The physical significance of this entropy change relates to the large increase in molecular order in going from the liquid to the crystalline state. The closer a solid gets to its perfect crystalline structure, the larger its decrease in entropy will be and the larger the resulting change in enthalpy will be.

The glassy slags which have so far been considered as thermal storage materials are noncrystalline solids which are properly regarded as being supercooled liquids in which the liquid-like disordered atomic arrangement has been "frozen into" the solid state.¹⁰ Glass formers such as silicates have complex molecular structures in the liquid state, and these liquids would require extensive atomic reorganization in order to assume the regular periodic structure characteristic of the crystalline state. In the absence of the ability of the glass-forming substance to undergo the necessary atomic rearrangement at a unique thermodynamic crystallization temperature, the liquid on cooling simply becomes increasingly viscous and eventually forms a solid glass.

If the solid slag in the vitreous state were to crystallize, its enthalpy and entropy would decrease. The decreases in the enthalpy and entropy would be, respectively, the latent heat and entropy of crystallization at the temperature at which devitrification occurred. However, the time required to attain this equilibrium structure completely

eliminates the possibility of slag crystallization in the proposed droplet heat exchanger. Freiman and Hench²² have observed periods of up to 24 hours for crystal nucleation alone to occur. The extremely rapid cooling rates in the droplet heat exchanger allow less than 5 seconds for the solidification process to occur (see Appendix C). Accordingly, the heat of fusion of the candidate slag compositions is not accessible and thermal storage is possible only in the form of sensible heat. A slag having a high specific heat is thus desirable.

The specific heat of the type of slag being considered is a function of both composition and temperature.²³ Multicomponent blast furnace slags containing SiO₂, Al₂O₃, CaO, MgO and trace quantities of other oxides have been studied at various times (see Ref. 23 and references therein). An empirical correlation which successfully predicts the specific heat of such slags was developed by Voskoboinikov.²⁴ He derived two equations for the mean specific heat, one for the temperature range of 20°-1350°C:

$$C_{20}^T = 0.169 + 2.10 \times 10^{-4}T - 2.77 \times 10^{-6}T^2 + 1.39 \times 10^{-10}T^3 \\ + 1.7 \times 10^{-5}T \left(1 - \frac{W_{CaO}}{\Sigma W_{oxides}} \right) \quad (3)$$

and another for the temperature range of 1350°C to 1600°C:

$$C_{20}^T = 1.5 \times 10^{-3}T - 4.78 \times 10^{-7}T^2 - 0.876 + 0.016 \left(1 - \frac{W_{CaO}}{\Sigma W_{oxides}} \right) \quad (4)$$

where C_{20}^T is the slag mean specific heat (cal/g/°C) in the temperature range 20°C to T, T is the temperature in °C, W_{CaO} is the weight fraction of CaO

and ΣW_{oxides} is the sum of the weight fractions of SiO_2 , Al_2O_3 , MgO and other oxides in the slag. The presence of CaO is seen to reduce the specific heat somewhat, but the effect is small. In essence, the specific heats of most slags of the type considered are approximately the same. At 1650°K these correlations predict a mean specific heat for Slag B of $0.292 \text{ cal/gm/}^\circ\text{C}$.

2.5 Thermal Conductivity

In the absence of published data on the high temperature thermal conductivity of the slag composition of interest, this property must, for the present, be estimated. Data on pure silica and various glasses indicate that the thermal conductivities of these media are similar, both in magnitude and temperature dependence.¹⁰ Data on MgO and CaO show conductivity values also similar to that of SiO_2 at temperatures of interest.⁷ Since the presence of impurities in an amorphous substance such as silica has a much smaller effect on thermal conductivity than in a crystalline substance,¹⁰ it is reasonable to assume that the thermal conductivity of the slag is approximately the same as that of pure silica, which varies from about $2 \text{ W/m}^\circ\text{K}$ at 800°K to $10 \text{ W/m}^\circ\text{K}$ at 1600°K , as shown in Fig. 3.⁷ This behavior includes the radiative (photon conduction) effect, which is important at high temperatures.⁸

2.6 Vapor Pressure

The vapor pressure of the storage medium must be very low to prevent contamination of the working gas in the droplet heat exchanger through evaporation of the droplets. Silica is the most volatile constituent of the slags considered here. Actually, the vapor phase above liquid SiO_2 contains hardly any SiO_2 at all.¹⁰ The vapor contains Si , Si_2 , Si_3 , O_2 and SiO , the

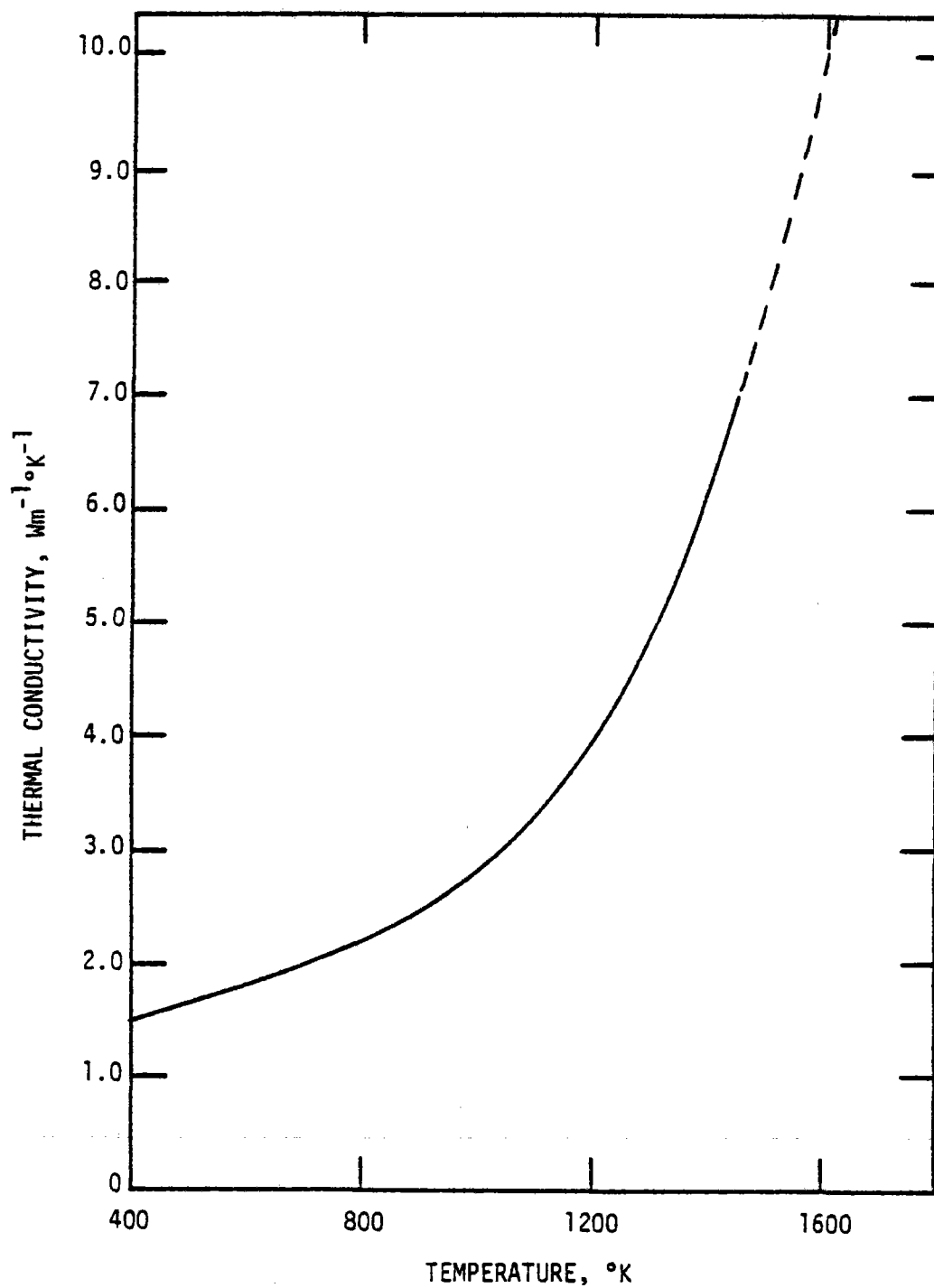


Fig. 3 Thermal conductivity of fused silica.⁷

latter two species being predominant. In other words, SiO_2 vaporizes by decomposing, primarily into SiO and O_2 . The other components of the slags (i.e., CaO , MgO and Al_2O_3) also vaporize by decomposing; however, the equilibrium partial pressures of their decomposition products are much lower than the partial pressures of SiO_2 decomposition.⁷ Thus it suffices only to consider the reaction:



where (ℓ) and (g) denote liquid and gas phases respectively. The partial pressures of SiO and O_2 at a given temperature can be determined from the equilibrium constant for the decomposition reaction at that temperature,²⁵ i.e.:

$$K = \frac{p_{\text{SiO}}^2 p_{\text{O}_2}}{a_{\text{SiO}_2}} \quad (6)$$

where p_{SiO} and p_{O_2} are the partial pressures (in atm) of SiO and O_2 respectively and a_{SiO_2} is the activity of SiO_2 , which in the absence of activity data for the slag composition considered here is assumed to be approximately equal to its mole fraction in the mixture.^{6,8} For Slag B, $a_{\text{SiO}_2} \approx 0.45$. The equilibrium constant, K , can be determined from the change in free energy, ΔG° , of the reaction, i.e.,²⁵

$$\ln K = - \frac{\Delta G^\circ}{RT} \quad (7)$$

Values of ΔG° are listed in standard reference tables.²⁶

If the molten slag is in a neutral atmosphere we can assume the stoichiometric constraint, i.e., $p_{SiO} = 2p_{O_2}$. Figure 4 shows a corresponding plot of p_{SiO} and p_{O_2} as a function of temperature over the range of 1500-2000°K.

At 1650°K the partial pressures are:

$$p_{SiO} = 3.45 \times 10^{-8} \text{ atm}$$

$$p_{O_2} = 1.73 \times 10^{-8} \text{ atm}$$

Compared to the 20 atm working gas pressure assumed in the droplet heat exchanger, these partial pressures are very small indeed, and contamination of the gas is minimal (see Appendix D).

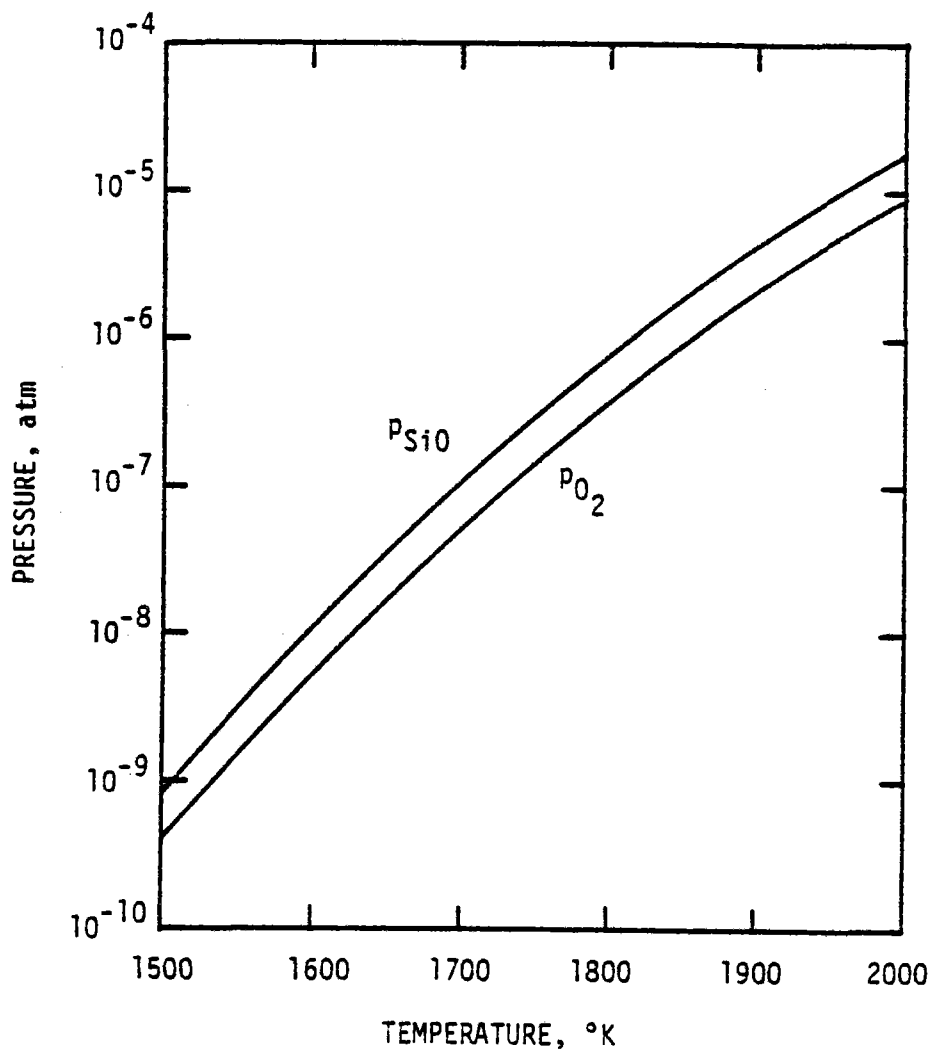


Fig. 4 Calculated vapor pressures of principal decomposition products of silica in a neutral atmosphere.

3.0 THE ENERGY STORAGE SYSTEM

3.1 Overview

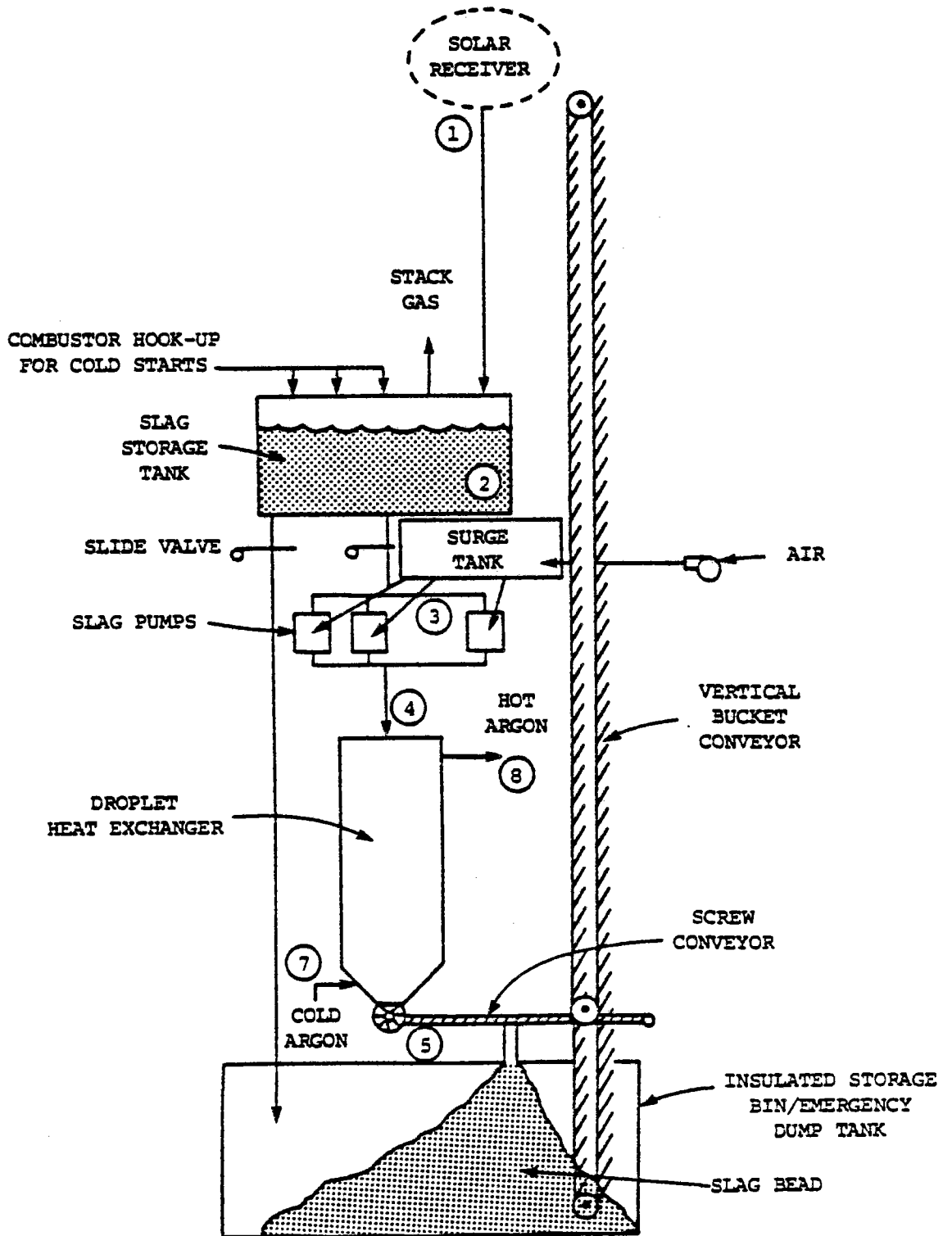
The capability of storing energy at the same high thermodynamic potential at which it is collected in the solar central receiver is a unique feature of the integrated system described here. Absorbing energy directly into the heat storage material in the solar central receiver leads to a storage method that is very easily integrated with the power cycle. Energy storage is accomplished by piping the molten slag to a refractory-insulated storage vessel. The material fills the vessel and from there is pumped to the droplet heat exchanger. Thus, a reserve of high, constant temperature molten slag is available at all times.

The principal components of the thermal storage system are shown in Fig. 5. It is characterized by three unique elements: a molten slag storage tank, gas-pressurized slag pumps and a slag droplet heat exchanger. The remaining elements shown in Fig. 5 are more conventional and can be related to existing technology in a relatively straightforward way. A preliminary design of the various components of the system is carried out in this section in order to size and cost the system.

3.2 General Considerations

The reference slag storage system is designed to deliver 23 MW_{th} to a 43% efficient Brayton cycle power conversion system,* to produce a net electrical power output of 10 MW_e . The size of the thermal storage system

*Conversion efficiencies of 50-52% would be possible by using an appropriate bottoming cycle.



82 06638

Fig. 5 Schematic of slag thermal energy storage system.
(Circled numbers refer to flow stations - see
Table 3.)

will depend on the number of hours of storage required; 1, 6, 15 or 48 hours for the examples considered.

The slag storage vessel, droplet heat exchanger and associated molten slag conduits, valves, pumps, droplet injectors, etc. must be designed with due regard for the physical and chemical stability of the materials in contact with the molten slag or the working gas at the high temperatures being considered. Much information relevant to this problem is already available from the highly developed technologies of the glass, steel and chemical process industries.²⁷

The slag flow conditions and power cycle gas flow conditions at key points in each of the two flow loops are indicated in Table 3 for the case of argon as the working gas. Some simplifying assumptions have been made in order to arrive at the most important design features with a minimum of effort. Specifically we assume no heat loss from the pipes connecting the storage tank and the droplet heat exchanger. Similarly, no viscosity-induced pressure drops are assumed for these same pipes; the actual viscosity and pumping power losses have been estimated and found to be very small compared to the hydrostatic pressure drops in these lines. Table 3 also includes estimates of the total tank slag storage mass and interior dimensions for a cylindrical geometry for the four reference storage times. The mass flow rate of slag is 27.8 kg/sec and the volume flow rate is approximately $9.6 \times 10^{-3} \text{ m}^3/\text{s}$. The flow rates are the same for all storage times.

The size of each of the major components will depend on the energy storage times and on the slag flow rates through the system. Additional assumptions must also be made about the rate at which these components will operate, their maintenance requirements, installation and operating

TABLE 3

Slag and Gas Flow Conditions for 23 MW(th), 10 MW(e) Plant

| | Station | Temp (°K) | Pressure (atm) | Mass Flow (kg/hr) |
|------|---------|--------------|-------------------|----------------------|
| SLAG | 1* | 1700 | 1 | 1×10^5 |
| | 2 | 1650 | 1 | 1×10^5 |
| | 3 | 1650 | 3 | 1×10^5 |
| | 4 | 1650 | 25 | 1×10^5 |
| | 5 | 980 | 1 | 1×10^5 |
| | 6 | 900 | 1 | 1×10^5 |
| GAS | 7 | 862 | 20 | 2.5×10^5 |
| | 8 | 1500 | 20 | 2.5×10^5 |

Tank Storage Masses and Interior Dimensions:

| Storage Time (hr) | Mass ⁺ (kg) | Height [‡] (m) | Diameter (m) |
|----------------------|---------------------------|----------------------------|-----------------|
| 1 | 9.6×10^4 | 4.5 | 3.5 |
| 6 | 5.8×10^5 | 7.3 | 6.3 |
| 15 | 1.4×10^6 | 7.5 | 9.8 |
| 48 | 4.6×10^6 | 7.5 | 17.6 |

*Refer to Figure 5 for flow station locations.

⁺Denotes useful storage media mass. An additional mass lies in the bottom 50 cm of the storage tank.

[‡]Includes 50 cm freeboard above the molten glass and 50 cm of unusable storage of slag below the drain port.

requirements and in some cases on the size and location of elements of the total power system lying outside of the storage system; for example, on the height of the solar receiver. Each of these items is considered for the components, as described below.

3.3 Molten Slag Storage Tank

A variety of refractory materials has been developed for use in the construction of glass-melting furnaces, blast furnaces and high temperature kilns.²⁷ In each case the particular choice of materials is dictated by the necessity to resist not only high temperatures and thermal shock but also chemical attack by corrosive glassy or metallic substances and reactive atmospheres.

Fused-cast refractories such as alumina-zirconia-silica (AZS) are widely used in the glass industry due to their excellent high temperature properties and resistance to corrosion by typical soda-lime glasses.²⁸ The steel industry uses high alumina firebrick and fusion castings or carbon blocks to line the interiors of blast furnaces.²⁷ Carbon is particularly attractive in this application due to its excellent high temperature structural properties, superior thermal shock resistance, resistance to corrosion by molten metals and some slags, non-wetting properties, ease of manufacture and low cost.²⁹ Carbon has not been widely used in the glass industry because of its tendency to discolor glass; however, in applications where discoloration is not important, such as in the manufacture of glass fiber, carbon has found some use.³⁰ Our own experience with melting basic slags in carbon crucibles is not encouraging. We have found that the carbon crucibles are significantly corroded by the type of slag considered here, probably as a result of the reaction of carbon with $MgSiO_3$, an intermediate compound present in the slag.

For our application it is necessary to use a refractory which is highly resistant to attack by the proposed basic slag (50% SiO₂, 30% CaO, 20% MgO). A number of studies of the corrosion of refractories by glasses and slags of various compositions³¹⁻³⁴ have indicated that the corrosiveness of such media increases rapidly with increasing basicity* and that the corrosion resistance of the refractories relates to their alumina-silica ratios, i.e., the refractories with the highest alumina contents possess the greatest resistance to slag corrosion. The AZS refractories widely used in the glass industry are prone to severe corrosion by basic slags due to their relatively high silica content.³⁴ The presence of silica in a refractory is detrimental to corrosion resistance because it promotes reaction products which form low melting point eutectics in the reaction layer at the surface of the refractory. Fused-cast alpha-alumina (99.3% Al₂O₃) has been found to have the highest corrosion resistance to basic slags.^{33,34} Alumina refractories in the presence of slags containing CaO and MgO form reaction layers composed of calcium hexaluminate (CaO·6Al₂O₃) and magnesium aluminate spinel (MgO·Al₂O₃), both of which are highly refractory, with melting points above 2100°K.³⁴ These reaction layers greatly retard further corrosion by the slag.

Corrosion of dense refractories such as fused-cast alumina by glasses and slags proceeds most rapidly at the junction of the surface of the melt and the refractory wall.³¹ This phenomenon is primarily a result of two effects: 1) downward currents induced at the wall by density increases in the melt resulting from the gradual solution of the refractory in the melt,

*Basicity is defined as the sum of the weight fractions of CaO and MgO divided by the sum of the weight fractions of SiO₂ and Al₂O₃.

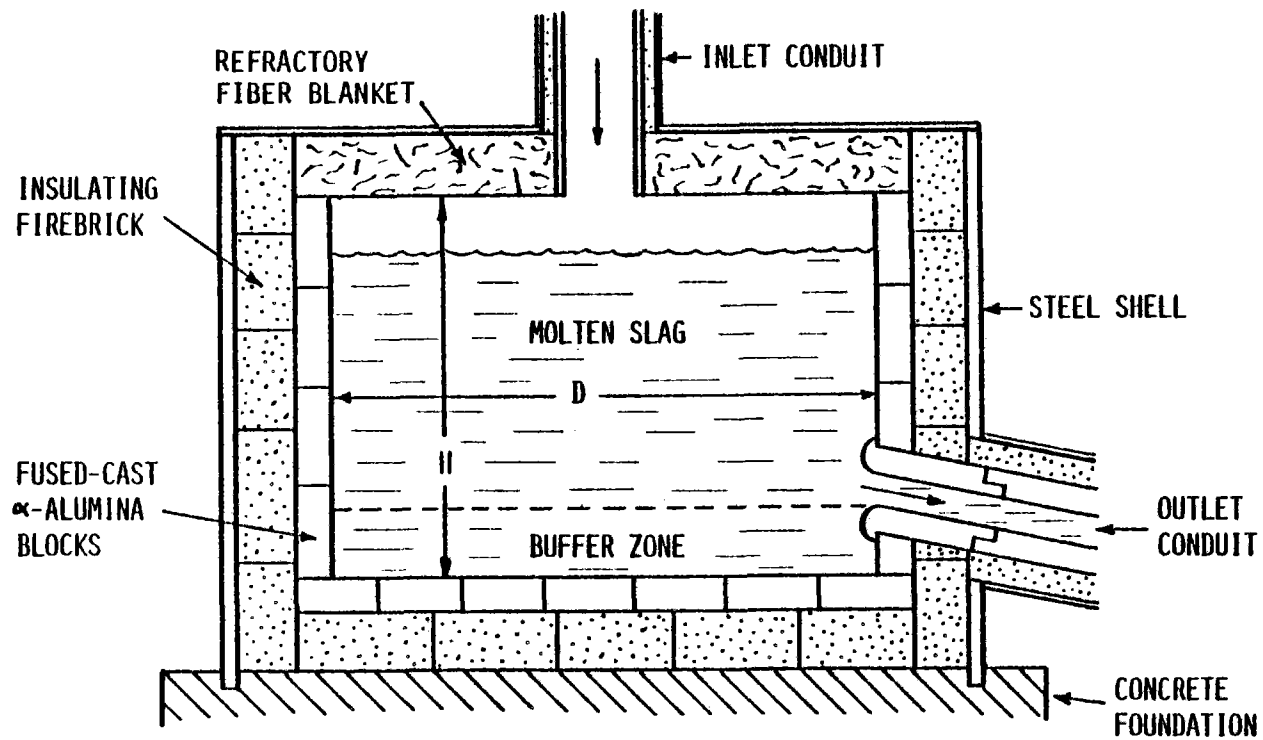
and 2) surface tension driven currents which result from the changes in surface tension brought about by the change in melt composition near the wall. These currents continuously bring fresh melt in contact with the wall, thus increasing the corrosion rate.

The slag corrosion test of Ref. 34 showed that at the melt line the corrosion of alpha-alumina by a slag of basicity 1.0 proceeds at the rate of ~1.5 mm per day at a temperature of 1800°K. Although no data for lower temperatures were presented, the results from other corrosion studies with soda-lime glasses³³ indicate that at 1650°K the corrosion rate is about one order of magnitude less than at 1800°K. For our tank life estimates we have conservatively estimated a corrosion rate of the alumina at the melt line of 0.2 mm/day at 1650°K. Corrosion of the totally submerged parts of the tank would proceed at a much lower rate.

In addition to its corrosion resistant properties, fused-cast alpha-alumina also exhibits high density, low porosity and high strength.³² Its thermal shock resistance is not as good as that of refractories containing silica²⁸ but is nevertheless adequate for its intended purpose.

It appears, thus, that fused-cast alpha-alumina is the most suitable refractory material, not only for the slag storage tank but also for much of the rest of the storage system. That is not to say that other materials would be entirely excluded. For example, the non-wetting property of carbon²⁹ may make it more suitable as the inner liner of the droplet heat exchanger cavity, where the slag is not in continuous contact with the wall.

Figure 6 illustrates a sketch of our proposed storage tank design, showing its principal components and dimensions. The tank has characteristics similar to a modern glass melter of the insulated type.



| STORAGE (hr) | 1 | 6 | 15 | 48 |
|--------------|-----|-----|-----|------|
| D (m) | 3.5 | 6.3 | 9.2 | 18.3 |
| H (m) | 4.0 | 6.8 | 7.5 | 7.5 |

Fig. 6 Cross-section of molten slag storage tank.

Construction would be similar for each of the 4 storage sizes considered: 1 hr, 6 hr, 15 hr and 48 hr storage. The tank is cylindrical in shape with a maximum fill height not to exceed 7 m of slag. The floor and side walls are lined with 30 cm thick fused-cast alpha alumina blocks (such as Carborundum Co.'s Monofrax Type A), fastened into place by high-alumina or chrome-alumina refractory mortar.*

Floor and wall insulation is provided by insulating firebrick. The type of firebrick, number of layers and thicknesses of the layers of firebrick are a function of the size of the storage tank and the temperature profile of the wall. Sufficient insulation is provided in each case to keep thermal losses below 1% of the total storage capacity over the rated storage period. Table 4 summarizes the parameters of the wall and floor insulation for each tank size.

Since the roof does not come into contact with the molten slag it does not need a slag resistant liner. The roof could be constructed entirely of insulating silica-alumina refractory fiber (such as Babcock & Wilcox Co.'s Kaowool) suspended from a roof cover plate. In all but the 48 hr tank a single layer of Kaowool of appropriate thickness is sufficient. The 48 hr tank uses a second layer of very low conductivity mineral wool. The roof insulation parameters are summarized in Table 5.

*Examples are Carborundum Co.'s Monofrax HMS laying cement (94% Al_2O_3) and Monofrax K laying cement (18.3% Cr_2O_3 , 75.4% Al_2O_3).

TABLE 4
Wall and Floor Insulation Parameters

| | | | | |
|--|--------|----------------------------|---------------|---------------|
| Storage time (hr) | 1 | 6 | 15 | 48 |
| Layers of insulation | 1 | 2 | 2 | 2 |
| Insulating firebrick | NA-26* | NA-26 K-23 [†] | NA-26 K-23 | NA-26 K-23 |
| Thermal conductivity [‡] W/(m°K) | 0.36 | 0.36 0.21 | 0.36 0.21 | 0.36 0.21 |
| Thickness of layer (m) | 0.3 | 0.15 0.3 | 0.23 0.45 | 0.3 1.22 |
| Heat loss (kW/m ²) | 1.4 | 0.68 | 0.46 | 0.19 |

*North American Refractories Co. (rated to 2600°F).

[†]Babcock and Wilcox Co. (rated to 2300°F).

[‡]Average over temperature range through layer.

TABLE 5
Roof Insulation Parameters

| | | | | |
|---------------------------------|----------|---------|---------|---------------------------|
| Storage time (hr) | 1 | 6 | 15 | 48 |
| Insulation | Kaowool* | Kaowool | Kaowool | Kaowool & Mineral Wool |
| Thermal Conductivity W/(m°K) | 0.22 | 0.22 | 0.22 | 0.22 0.04 |
| Thickness (m) | 0.23 | 0.45 | 0.76 | 1.07 0.18 |
| Heat Loss (kW/m ²) | 1.2 | 0.63 | 0.39 | 0.18 |

*Babcock and Wilcox Co. (rated to 2600°F).

The exit port is located 50 cm above the floor level to provide a buffer layer of solidified slag which protects the floor from excessive thermal shock and erosion during initiation of tank fill. This exit port is assembled from fused-cast alpha-alumina conduit material, although it may be necessary to use high chromic oxide content material such as Carborundum's Monofrax K, which has been demonstrated to have excellent resistance to erosion by flowing glasses. The resistance of high chrome refractory to erosion by flowing basic slags is not well documented, however, and must be established by experimentation.

An internal diameter of the exit port and conduit of 25 cm results in an average slag exit velocity of 0.2 m/sec. This low velocity is necessary to minimize erosion of these components. Note that the exit port protrudes into the melt to reduce the likelihood that erosion of the inlet will eat into the tank liner material.

The choice of 7 m of slag as the maximum fill height is dictated by tank lifetime considerations; above this height increased erosion between the tank floor pavers is likely to occur, drastically shortening floor life and increasing replacement costs. The tank is filled to within 50 cm of the roof to avoid hole drilling into the roofing insulation.³⁵

Based on our earlier estimate of a slag corrosion rate of 0.2 mm/day it is estimated that the 30 cm thick fused-cast α -alumina blocks will have a typical lifetime of 4 years at the melt line and perhaps twice that everywhere else. These figures are similar to the service lives of some glass melting tanks in current use. In the glass industry a worn out tank is either relined or completely dismantled and replaced by a new tank. For our economic analysis (Section 4.0) we have assumed an average liner life of 6.5 years.

Several natural gas-fired combustor inlets are integrated into the storage tank ceiling to preheat the tank in the case of a dead cold start, and thus avoid thermal shock damage to the walls. Specifically, the combustors should be capable of raising the tank wall temperature by $\sim 1200^{\circ}\text{K}$ over a period of 24 hours. The heat capacity of the tank includes 50 cm of slag on the bottom of the tank and sufficient mass in the walls to account for the establishment of a steady temperature profile in the walls as the preheating process continues. If the insulation is good, then only the heat capacity of the wall liner material is important. This calculation leads to a total heating requirement of 91 GJ, 300 GJ, 550 GJ and 1.18×10^3 GJ for the four storage times, respectively. The exhaust stack can be the slag inlet conduit itself. In this manner preheating of this conduit and the solar receiver cavity can also be accomplished at the same time. The gas-fired preheater apparatus has not been included as part of the permanent plant since mobile tank preheating services are available on a contractual basis³⁶ and since dead cold starts are likely to be infrequent. The glass industry makes wide use of such mobile preheater services to avoid the capital cost of a permanent installation.

The entire tank is enclosed in a reinforced steel shell which provides structural strength to the tank walls. The construction envisioned at this time is a plain cylindrical shell which carries the circumferential hydrostatic head load in tension and acts as a retaining wall for the tank liner and insulation. A shell thickness of 12.5 mm is more than adequate for even the largest tank. Columns of I-section located at regular intervals around the circumference carry the roof load. The columns are braced in the circumferential direction by the shell acting as a shear panel and in the radial direction by the horizontal girders which support the

roof. In the case of the largest tank these roof girders are built-up trusses. The entire assembly is supported by a reinforced concrete foundation of appropriate thickness and a diameter which distributes the load to a value below 192 kPa (4000 psf). This represents the soil bearing strength used in all thermal storage concept evaluations.

3.4 Storage Tank Feed Pipe

The solar receiver is located directly above the storage tank so that the glass melt will stream down a feed pipe directly to the tank without the use of pumps. The feed pipe is assumed to be 10 meters high and 80 cm inner diameter, large enough so that the slag does not touch the pipe walls and so that the radiative flux per unit area at the walls is at a tractable level. The pipe is lined with 10 cm of graphite surrounded by 30 cm of insulating firebrick (NA-26*) with a structural steel outer shell. The weight of the feed pipe is assumed to be borne by the receiver tower and is not included in the strength of the pipe shell. The shell is simply strong enough to transfer the weight of the insulation liner to the tower, at intervals along its height.

3.5 Emergency Slag Dump

A catchment tank is located below the storage tank to receive the entire contents of the storage tank in case of an emergency failure at any point in the slag flow loop. The slag will form thermally stressed, solid filaments by quick cooling in water flooded into the dump tank. These filaments can be easily shattered with a mechanical crusher so that the resulting fines can be recycled to the solar receiver at start-up. The

*North American Refractories Co. (rated to 2600°F).

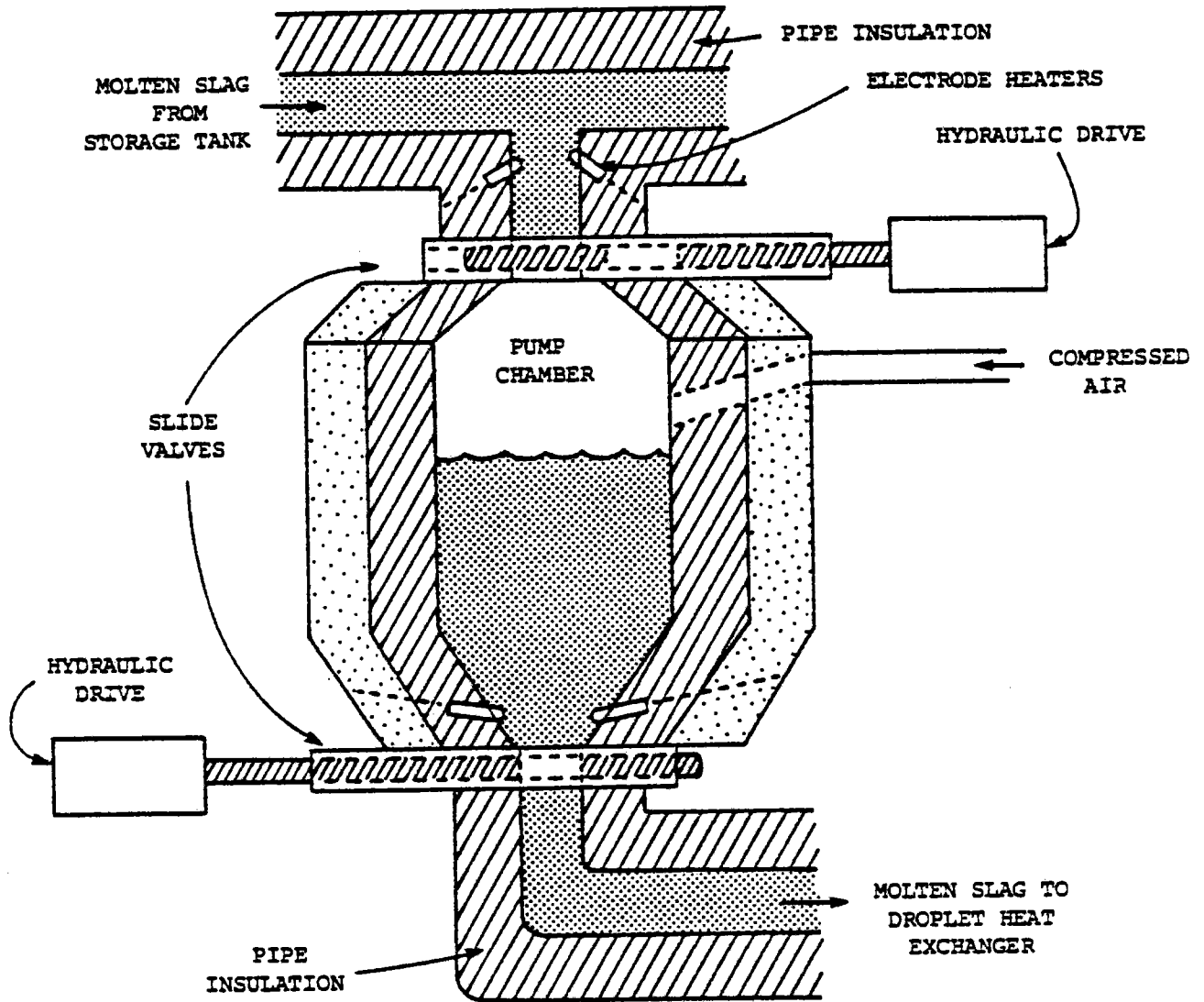
crusher, water supply connection, pipes and pumps complete this component subsystem. Approximately 450 m³ of water are needed to cool the contents of the 1 hour storage tank to 373°K (boiling water); larger amounts of water are required in direct proportion to the storage times.

3.6 Molten Slag Pumps

A sketch of the reciprocating molten slag pump design assumed in this analysis is shown in Fig. 7. The pump is operated by injecting slag under its own head from the storage tank into the pump chamber, which is at ambient atmospheric pressure. The top valve is closed and air is pumped into the chamber under pressure. Then the bottom valve is opened to eject the slag into the pipe leading to the droplet heat exchanger, where the slag is pumped under pressure through the injector nozzle plate of the heat exchanger. Since these pumps are operated in a batch mode, several are required so that some are filling while others are emptying, in order to yield a continuous flow of slag.

The sizes of currently available slide valves³⁷ limit the flow rate of slag from any single pump. The size of the pump chamber determines the length of fill and empty times, and hence the thermal cycling which each pump will encounter. These cycling times affect the replacement schedule and corresponding costs for the pumps. An air compressor, surge tank to supply a reservoir of gas at the proper pumping pressure, and valves for exhausting the air to ambient pressure every half cycle complete this component subsystem.

The reference pump design assumes that the full pump cycle time is 5 minutes; this is not an optimized value but was chosen simply for illustrative purposes. The peak pump pressure required is 25 atm (see Appendix E). The largest diameter slide valve available has a 11.0 cm



82 06639

Fig. 7 Cross-sectional view of reciprocating molten slag pump and inlet and exit pipes.

throat diameter;³⁷ we further limit the flow speed through the valve to 0.2 m/s in order to limit the valve erosion. The resulting mass flow rate through one pump is 5.5 kg/sec. Thus, approximately 5 active pumps are needed to sustain the total slag flow required. At least ten pumps would be needed, considering half of them would be emptying at any given time. The active volume of each pump chamber must be 500 liters, giving a characteristic dimension for a cylindrical pump of 86 cm height and diameter. The freeboard space at the top of the pump chamber is assumed to be 25 cm. The compressed air requirements are on the order of 5.5 m³/min (200 cfm) at standard pressure and temperature for the entire group of 5 active pumps. The pumps are lined and insulated with the same materials used in the slag storage tank (30 cm α -alumina liner; 30 cm NA-26 insulating firebrick), with the addition of electrode heating elements located above each entrance and exit valve to reliquify the slag, if necessary, when it is to start flowing.

3.7 Droplet Heat Exchanger

The droplet heat exchanger consists of a single, insulated pressure vessel. One possible configuration is illustrated in Fig. 8. The pressurized molten slag is injected into the heat exchanger through a refractory-metal nozzle manifold pierced with a multitude of small holes. The resulting liquid streams can be made to break up into a series of uniform droplets by pulsing the feed pressure at the appropriate frequency, as discussed in Appendix B. The droplets fall through the heat exchanger cavity, giving up their heat to a suitable inert working gas by conductive, convective and radiative processes. The heated gas is then used as the working fluid in the high temperature heat engine.

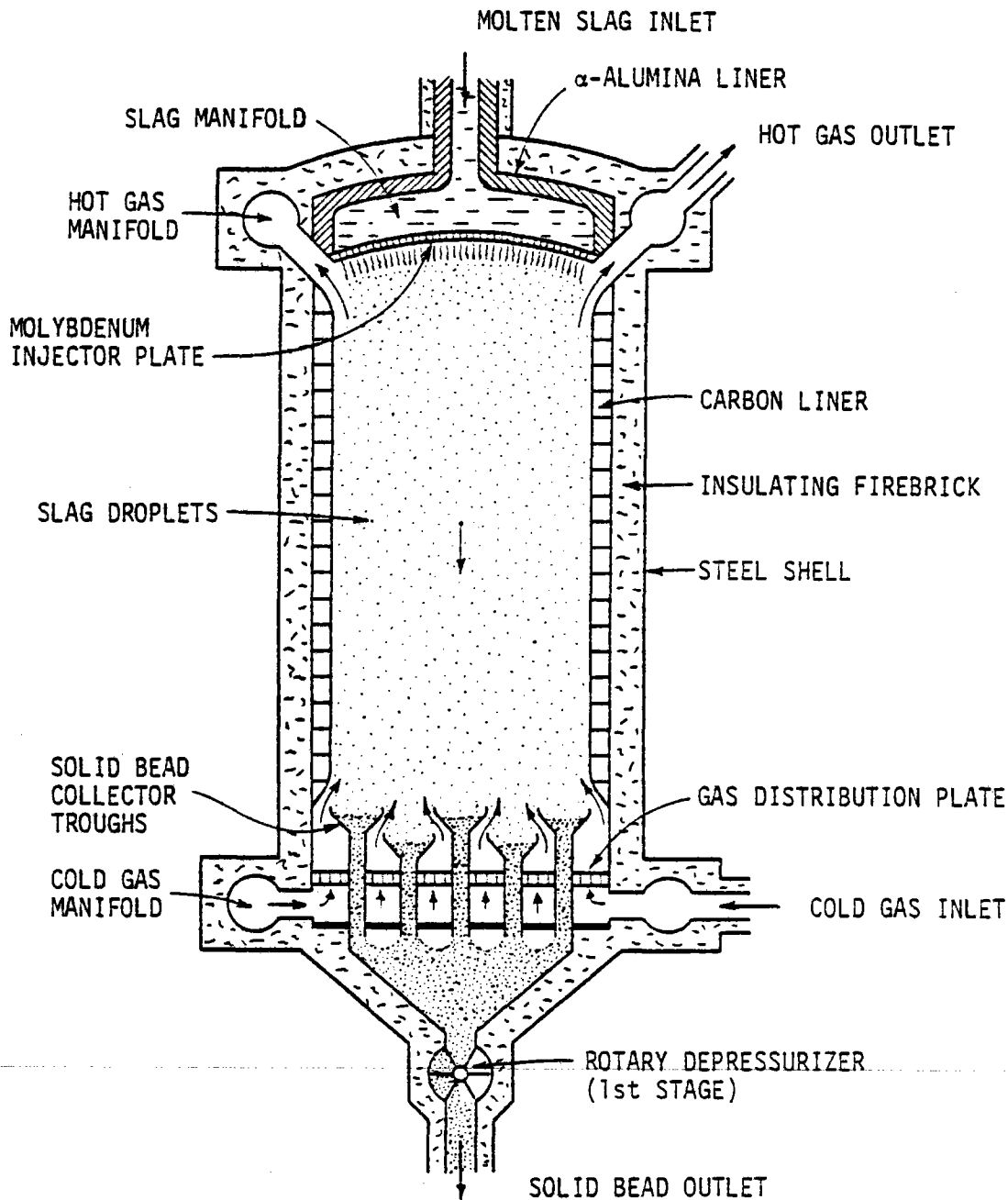


Fig. 8 Schematic of high temperature droplet heat exchanger.

A full, one-dimensional, two-phase flow heat transfer analysis of the droplet heat exchanger is presented in Appendix C, together with baseline design calculations for argon as the working gas. The design for a droplet heat exchanger using nitrogen would be similar, although the overall dimensions would be somewhat different. Capital costs are not very sensitive to the type of gas used.

The droplet heat exchanger column for heating argon at 20 atm to 1500°K is 6.5 meters of active height with an inner diameter of 3 meters. A molybdenum nozzle plate is used to form the 1 mm droplets of slag which fall through the upwelling flow of argon. The 0.5 m deep slag reservoir above the nozzle plate is lined with 30 cm of fused-cast α -alumina. The walls of the heat exchange chamber are lined with graphite bricks 23 cm thick, and these are backed with 45 cm of insulating firebricks (Babcock & Wilcox Co., type K-23, $k=0.21$ W/(m°K)). The outer steel pressure shell is 2.5 cm thick.

The droplets are assumed to be free of the walls except for occasional splashing; slag does not wet carbon blocks under clean conditions. The droplets cool to a non-sticky solid state (980°K) by the time they reach the bottom of the column. A rotating pressure lock, as sketched in Fig. 8 and described in Appendix F, moves the solid slag pellets to a gas recovery chamber and thence through a second rotating pressure lock to a horizontal conveyor belt, which either transfers them to a vertical conveyor or to an intermediate storage bin. The net loss of argon through the tandem rotating pressure locks is approximately 0.67 kg/hr or 2.7×10^{-6} of the flow of gas through the heat exchanger (see Appendix F).

The nozzle plate must be a reinforced structure, thin enough near the 0.4 mm dia nozzle orifices to allow small droplets to emerge through nozzles with length to diameter ratios on the order of 5, yet thick enough away from

the nozzles to sustain the necessary pressure drop of 5 atm across the nozzles. At 1650°K, the tensile strength of molybdenum is 15 kpsi. A flat nozzle plate 3 m in diameter would have to be 4 cm thick and would weigh approximately 3000 kg. It is likely that using a curved honeycomb cellular design the weight of this component can be reduced to ~1000 kg. A more detailed design of this element is clearly needed in order to obtain an accurate estimate of its mass and cost.

3.8 Temporary Slag Storage Bin

The emergency dump tank discussed earlier will normally operate as a temporary insulated storage bin to keep the solid slag beads at approximately 900°K during periods of no insolation. Maintaining the bead temperature at this value will minimize the thermal shock to the solar receiver when the beads are carried to it for a "cold" start. (Under normal sunlight conditions, the beads would be returned directly to the receiver at approximately their discharge temperature, 980°K, from the heat exchanger). This bin will require a gas preheater in order to counteract thermal losses incurred over very long storage times. The preheating can occur by locating the combustor at the base of the enclosed vertical conveyor lifting the bead from the storage bin to the receiver. The enclosure of the conveyor will act as the exhaust stack under these circumstances, giving the beads a relatively long residence time in the hot gas stream, and eliminating the need for a secondary heat exchanger (e.g., otherwise a small fluidized bed heater might be required). This approach does have some penalties; namely, the combustor temperature must be relatively low, in order not to overheat the vertical conveyor system. However, the conveyor acts as a co-flowing heat exchanger to help compensate for the relatively low temperature difference between the gas and the beads.

For example, using a combustion gas temperature of 1370°K, a combustion gas flow of 1200 m³/s (2.5×10⁶ cfm) is required in order to raise the bead temperature to 900°K from 300°K, the long term storage temperature. A lower combustion flow requirement could be invoked if the power system were started up gradually, instead of at full power.

3.9 Vertical Bucket Conveyor

This conveyor lifts the beads to the top of the solar receiver from the temporary storage bin, at the lowest point, and normally from the base of the droplet heat exchanger tower. A total height of approximately 40 m is assumed. The entire conveyor is mounted inside of an insulating housing designed to operate at an interior temperature of 980°K. Vents are provided at the top to regulate the internal temperature and to exhaust the stack gases when the combustors (i.e., preheaters) are being used. The conveyor motors are attached outside of the housing.

3.10 Solar Central Receiver

Although the solar receiver is not, in the strict sense, a part of the thermal energy storage system, and we do not develop any cost data for it in this report, it is nevertheless included here for the sake of completeness.

The solar receiver is an important component of the proposed solar thermal power plant and energy storage system. It is here that the solid slag beads are melted and heated to the desired temperature for storage and subsequent use in the direct contact droplet heat exchanger. The design considerations for an optimum receiver geometry are only exploratory at this stage. One conceptual solar receiver design is shown schematically in Fig. 9. The receiver is a vertical cylindrical cavity having an axial slot aperture which faces a stepped, north-field heliostat. The solar flux is

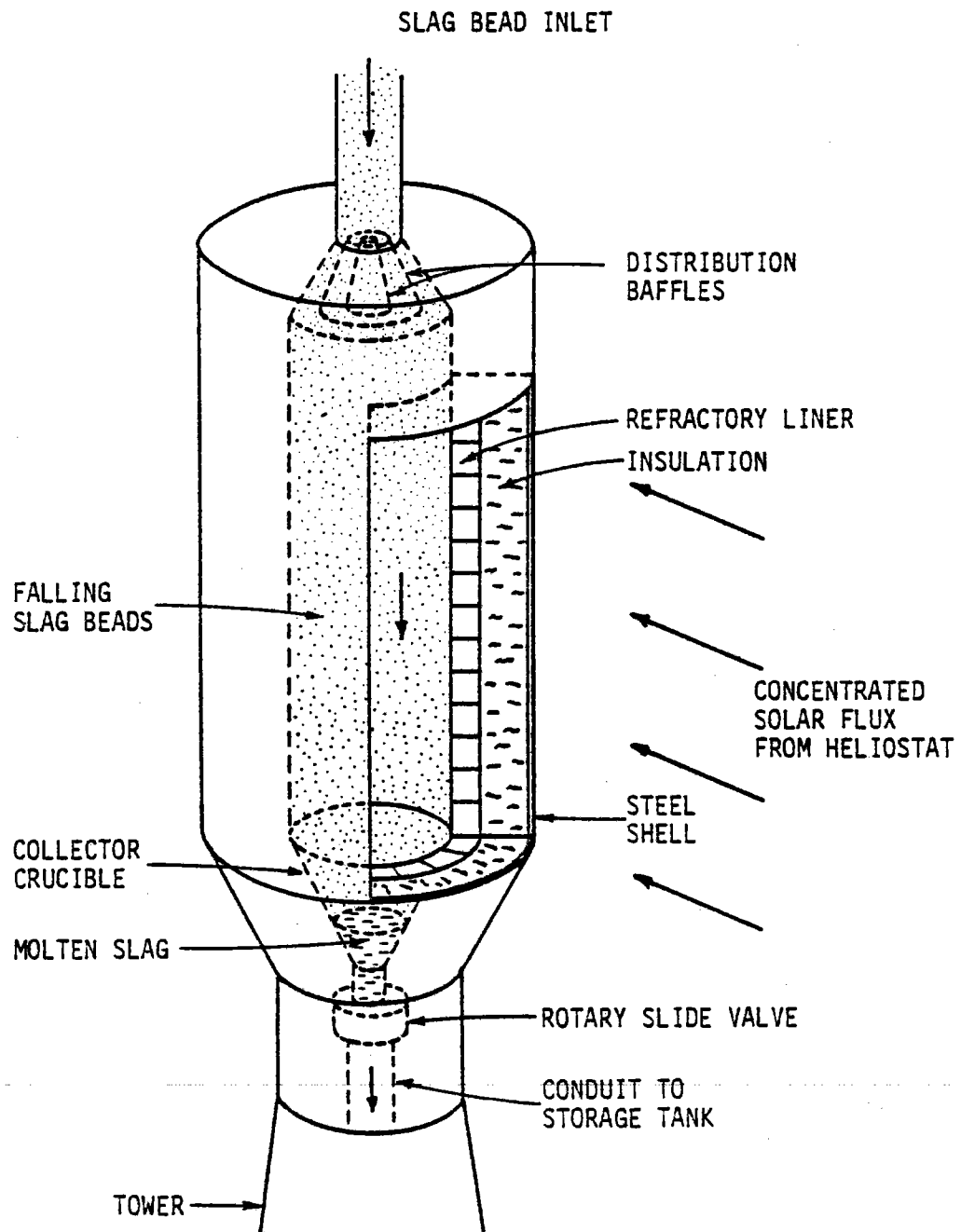


Fig. 9 Schematic of conceptual design of solar receiver for melting slag beads.

concentrated into a vertical rectangular spot having dimensions the size of the cavity opening and enters the cavity in a near horizontal direction. The solar receiver cavity would be approximately 3 m inside diameter and 12 m high. (See Appendix G.) With a slot 2.1 m wide the required concentration ratio of the heliostat would be approximately 1400, which is attainable with present technology.

The solid bead aggregate is delivered by a bucket conveyor to a suitable hopper at the top of the cavity. The beads are introduced into the cavity as a uniformly distributed dispersion and fall through the cavity at terminal velocity. During their downward transit the beads are heated to the desired temperature by a combination of direct solar flux and reradiation from the cavity walls. Through suitable choice of design parameters the beads can be heated beyond their melting point. The molten beads fall into a pool of molten slag in a conical refractory crucible located below the receiver cavity. The melt flows out of the crucible at a controlled rate through a high-temperature rotary slide valve³⁷ and down an insulated refractory conduit into the thermal storage tank below. (This conduit was described in Section 3.4.)

The solar receiver cavity is lined with a suitable high-temperature oxidation-resistant and thermal shock resistant refractory. A carbon-based composite material has been developed which may be ideally suited to this purpose.³⁸ Insulation is provided by insulating firebrick or fiber refractory material, such as Kaowool.

In the case of loss of insolation due to a sudden overcast or nightfall, the injection of beads at the top of the solar receiver would automatically stop and the molten material in the crucible would be emptied into the storage vessel. An insulated shutter (not shown, for clarity)

would close off the cavity aperture to minimize heat loss from the hot cavity. At re-start, cold beads from the solid slag storage bin would be preheated to the required inlet temperature in the combustion heated bucket conveyor system. The receiver cavity would be preheated to operational temperature by the solar flux prior to resumption of bead delivery. The slide valve at the bottom of the melt crucible would remain closed until a prescribed level of molten slag accumulated in the crucible. The rotary slide valve would open gradually to establish the required slag flow rate into the storage tank. The feed rate of the solid bead aggregate at the top of the receiver would then be adjusted to result in steady state operating conditions.

The performance of the solar receiver has been analyzed using a simple radiative exchange model which neglects scattering by the beads. A description of the model and some sample results are presented in Appendix G.

4.0 ECONOMIC ANALYSIS

4.1 Methodology

The techniques developed by Stearns-Roger Services, Inc.² for costing thermal storage systems for SERI are applied to the high temperature slag thermal storage system described in the previous sections of this report. The chief feature of the cost calculation is a separation of component costs into energy related costs and power related costs, the latter depending on the rate at which thermal energy is to be extracted from the storage unit. Operations and maintenance costs and replacement costs also are included. The cost analysis is carried out in terms of the capital cost per kW-hr of thermal storage and in terms of the present worth of revenue requirements (PWRR). Those storage concepts which have the lowest PWRR values are the most economical. The results of the PWRR calculations for the molten slag storage concept are compared to the PWRR values for competitive thermal storage concepts. The precise format for these calculations is indicated in Table 6.

To summarize, the price year for cost information is 1980, the first year for commercial operation is 1995, a factor of 1.95 is used as a multiplier on direct capital costs in the field to arrive at total capital investments, a factor of 1.8 is used as a multiplier on equipment cost to arrive at direct field costs for constructed items, a fixed charge rate of 0.17 is used, which corresponds to a rate of return on capital of 10%, and the annual escalation rate is 7% which covers general inflation and escalation of capital costs, operating costs and maintenance costs. We have also used the Stearns-Roger values of annual O&M costs equal to 3% of the capital investment, since more accurate values are not available.

TABLE 6

Formulae Used in Cost Analysis²

$$\text{Material Cost} \equiv \text{MC} = \text{CP} + \text{CE}^*$$

$$\text{Total Material Cost} \equiv \text{TMC} = 1.8 \times \text{MC}$$

$$\text{Total Installed Cost} \equiv \text{TIC} = \text{TMC} + \text{SC}^*$$

$$\text{Total Capital Investment} \equiv \text{CI} = 1.95 \times \text{TIC}$$

$$\text{Total O\&M} \equiv \text{TOM} = 0.03 \times 1.95 \times \text{TMC}$$

$$\text{Total Energy Costs/year} \equiv \text{TEC} = (2.28 \times 10^5 \text{ kW}\cdot\text{hr}) \times \$0.035/\text{kW}\cdot\text{hr}$$

$$\text{Total Chemical Costs (argon)} \equiv \text{TCC} = 4700 \text{ kg/yr} \times \$13.6/\text{kg}$$

$$\text{Total FYVC} = \text{TOM} + \text{TEC} + \text{TCC}$$

$$\text{Total Replacement Cost} \equiv \text{TRC} = 1.8 \times \text{RC}^*$$

$$\text{Present Worth Replacement Cost} \equiv \text{PWRC}$$

$$\text{where PWRC} = \text{TRC} \times \sum_{k=1}^n (0.9727)^{kx^*}$$

$$\text{Present Worth Revenue Requirement} \equiv \text{PWRR}$$

$$\text{where PWRR} = 1.6(\text{CI}) + 20.1 (\text{FYVC}) + \text{PWRC}$$

*CE = Energy Related Costs

CP = Power Related Costs

SC = Storage Medium Cost

RC = Replacement Costs

x = Replacement Interval (years)

n = Int(30/x-1) = Integral number of replacements in 30 year plant lifetime.

4.2 Component Capital Costs

The material unit prices used in the economic analysis are listed in Table 7. These reflect current industry prices adjusted to 1980 dollars by assuming a 10%/year escalation rate. The units are those commonly used in industry. The unit price for the slag storage medium is based on field mixing and processing of the raw materials listed in Appendix A.

A breakdown of component costs for the storage tank, for each of the four storage times, is shown in Table 8. A similar breakdown of power related costs is listed in Table 9.

Table 10 lists each of the main component subsystem costs and identifies these as primarily energy or power related cost categories. In addition, Table 10 indicates the costs of the storage media for each of the four storage times; these values are quite low compared to all other forms of storage media, including rock storage. Replacement costs are also computed for the alpha-alumina liners of the storage tanks, high temperature slag pipes, slag pumps and for the droplet heat exchanger injection reservoir; the replacement of all liners is assumed to occur every 6.5 years. The pump compressor engine also requires new piston rings every 12 months, but the cost relative to the refractories is negligible. Some chemicals are consumed or lost; notably, the working gas from the power cycle leaks slowly from the tandem pressure locks at the base of the droplet heat exchanger. The loss rate is estimated to be approximately 0.67 kg/hour for argon and the cost of the argon loss is included in the calculation of present worth revenue requirements. Table 11 provides a breakdown of various costs as computed by the formulae of Table 6.

TABLE 7
Material Unit Costs*

| <u>Material</u> | <u>Cost</u> | <u>Reference</u> |
|--------------------------------|-------------------------|---|
| α -Alumina (fused-cast) | \$3400/ton ⁺ | Carborundum Co. |
| Firebrick: NA-26 | 0.36/lb | North American Refractories |
| K-23 | 0.33/lb | Babcock & Wilcox |
| Kaowool | 3.00/bd-ft | Babcock & Wilcox |
| Steel | 0.65/lb | Stearns-Roger ² |
| Concrete (reinforced) | 105/yd ³ | Stearns-Roger ² |
| Carbon (Graphite) | 1.00/lb | Chemical Marketing Reporter |
| Molybdenum | 24/lb | Penberthy Electromelt Int'l ³⁶ |
| Slag | 0.023/lb | Chemical Marketing Reporter |

*Costs are given in 1980 dollars. An escalation rate of 10%/year was assumed to compute 1980 prices from current (1982) prices.

TABLE 8
Storage Tank Costs (in 1000\$)

| | Energy Storage Times | | | |
|-------------------------|----------------------|-------------|--------------|--------------|
| | <u>1 hr</u> | <u>6 hr</u> | <u>15 hr</u> | <u>48 hr</u> |
| α-Alumina | 263 | 742 | 1271 | 2684 |
| Insulating Firebrick | 15 | 50 | 131 | 615 |
| Kaowool Roof Insulation | 4 | 21 | 82 | 413 |
| Steel Shell | 15 | 38 | 66 | 152 |
| Concrete Foundation | <u>1</u> | <u>3</u> | <u>9</u> | <u>52</u> |
| Total Cost | 298 | 854 | 1559 | 3916 |

TABLE 9
Power-Related Costs (in 1000\$)

| <u>Component</u> | <u>Cost</u> |
|--------------------------------|-------------|
| Droplet Heat Exchanger | 270 |
| Slag Pumps | 570 |
| Air Compressor | 70 |
| Receiver-to-Storage Feed Pipe | 25 |
| Storage-to-Heat Exchanger Pipe | 163 |
| Bucket Conveyor + Drive Motor | <u>30</u> |
| Total Cost (CP) | 1128 |

TABLE 10
Component Costs for High Temperature Slag Thermal Energy Storage System
(in 1000\$)

| | Hours of Storage | | | |
|---------------------------------|------------------|-------------|--------------|--------------|
| | <u>1 hr</u> | <u>6 hr</u> | <u>15 hr</u> | <u>48 hr</u> |
| ENERGY-RELATED COMPONENTS (CE) | | | | |
| Slag Storage Tank | 298 | 854 | 1559 | 3916 |
| Temporary Storage Bin | 50 | 132 | 221 | 467 |
| Total Cost (CE) | 348 | 986 | 1780 | 4383 |
| STORAGE MEDIA (SC) | | | | |
| Total Slag Cost | 5 | 28 | 69 | 225 |
| REPLACEMENT COSTS (RC) | | | | |
| (α -Alumina @ 10 years) | 487 | 965 | 1494 | 2907 |
| POWER-RELATED COSTS (CP) | 1128 | 1128 | 1128 | 1128 |

TABLE 11
Cost Calculations (in 1000\$) for 23 MW(th) Slag Storage System

| | Energy Storage Times | | | |
|------|----------------------|-------|-------|-------|
| | 1 hr | 6 hr | 15 hr | 48 hr |
| CE | 348 | 986 | 1780 | 4383 |
| CP | 1128 | 1128 | 1128 | 1128 |
| MC | 1476 | 2114 | 2908 | 5511 |
| TMC | 2657 | 3805 | 5234 | 9920 |
| SC | 5 | 28 | 69 | 225 |
| TIC | 2662 | 3833 | 5303 | 10145 |
| CI | 5191 | 7475 | 10342 | 19782 |
| TOM | 155 | 223 | 306 | 580 |
| TEC | 8 | 8 | 8 | 8 |
| TCC | 64 | 64 | 64 | 64 |
| FYVC | 227 | 295 | 378 | 652 |
| RC | 487 | 965 | 1494 | 2907 |
| TRC | 877 | 1737 | 2689 | 5233 |
| PWRC | 2283 | 4521 | 7000 | 13621 |
| PWRR | 15151 | 22411 | 31145 | 58377 |

The results of the economic analysis of the molten slag storage system are summarized in Table 12, where they are compared to similar figures for alternative storage schemes.² It should be noted that the figures for the alternative concepts were adjusted from Ref. 2 (Phase 2) to reflect 10 MW_e output, i.e., the figures in Ref. 2 were multiplied by 10/112. This linear scaling underestimates the costs of the alternative concepts because the cost of a storage system increases more slowly than the power level. Unfortunately, due to the lack of cost data as a function of power, the degree of underestimation of the costs of the other concepts could not be determined.

Cost data for 48 hour storage for the alternative storage concepts were not available either. Accordingly, for approximate comparative purposes, Table 12 includes 48 hour data linearly extrapolated from 15 hour data. Note that the linear scaling overpredicts the cost for molten slag at 48 hours and thus both the draw salt and air/rock storage costs are also overpredicted (i.e., the true costs are less).

By far the costliest item in the energy related category is the fused-cast α -alumina liner material used in the storage tanks. This material also accounts for more than one-sixth of the power related costs. Fused-cast α -alumina is a specialty item produced in small quantities and is therefore expensive. Current prices (1982) are in the \$6500/Ton* range, however, an estimate of \$4100/Ton was quoted by the Carborundum Co. for amounts sufficient for the 1 hr tank. Larger orders would bring about further reductions in price. We have used the \$4100/Ton (\$3400/Ton in 1980 dollars) figure for all four storage times. A 50% reduction in the price of

*The unit of Ton, as used here, is equivalent to 2000 lb.

TABLE 12
Thermal Storage Economic Evaluation for the High Temperature Slag Storage System

| STORAGE CONCEPT (10 MW _e) | COST \$1000 (1980) | | | | | | CI/kW·hr(th) |
|---------------------------------------|--------------------|-------|-------|--------|------|--------|--------------|
| | CE | CP | MEDIA | CI | FYVC | PWRR | |
| <u>1 hr</u> | | | | | | | |
| High Temperature Slag | 348 | 1,128 | 5 | 5,191 | 227 | 15,151 | 226 |
| Draw Salt* (2-Tank, Int. Insul.) | 69 | 330 | 97 | 1,591 | 60 | 3,742 | 69 |
| Air/Rock* | 132 | 659 | 40 | 2,855 | 103 | 6,642 | 124 |
| <u>6 hr</u> | | | | | | | |
| High Temperature Slag | 986 | 1,128 | 28 | 7,475 | 295 | 22,411 | 54 |
| Draw Salt* (2-Tank, Int. Insul.) | 314 | 476 | 582 | 3,908 | 132 | 8,906 | 28 |
| Air/Rock* | 207 | 620 | 115 | 3,129 | 161 | 8,241 | 18 |
| <u>15 hr</u> | | | | | | | |
| High Temperature Slag | 1,780 | 1,128 | 69 | 10,342 | 378 | 31,145 | 30 |
| Draw Salt* (2-Tank, Int. Insul.) | 638 | 588 | 1,454 | 7,135 | 234 | 16,119 | 21 |
| Air/Rock* | 313 | 843 | 244 | 4,621 | 264 | 12,555 | 13 |
| <u>48 hr</u> | | | | | | | |
| High Temperature Slag | 4,383 | 1,128 | 225 | 19,782 | 652 | 58,377 | 18 |
| Draw Salt** | 2,042 | 588 | 4,653 | 18,305 | 749 | 44,343 | 16 |
| Air/Rock** | 1,002 | 843 | 781 | 7,999 | 845 | 29,779 | 7 |
| High Temperature Slag** | 5,696 | 1,128 | 225 | 24,391 | 791 | 75,025 | 22 |

*Figures adjusted from Ref. 2 (Phase 2), Tables 4-6 to 4-8): Multiplied by (10/112) to reflect 10 MW_e output. This linear scaling underestimates the costs of these concepts.

**Linearly scaled from 15 hour data (overpredicts all costs).

α -alumina would result in approximately a 25% reduction in CI and an approximately equal reduction in PWRR for the larger storage systems. If this cost reduction were realizable, the cost per kW-hr of the molten slag system for 15 hour storage would be approximately the same as that of the draw salt system. For storage exceeding 48 hours the molten slag system would be more economical.

Another very costly item is the group of 10 slag pumps, which accounts for more than half the power related costs. The reason for this high cost lies in the high temperature slide valves, each of which costs ~\$19,000. Twenty such valves are needed, constituting 66% of the cost of the present pumping system design. Considerable cost reductions could be effected by reducing the number of pumping chambers and consequently the number of valves. This would lead to an increased flow velocity through the valve throats and would thus necessitate more frequent replacement of the alumina slide gates and nozzles. However these replacement costs would be small compared to the potential capital savings of reducing the number of valves. Reductions of 20-25% in the power related costs should be possible by such measures.

It should be strongly stated that the cost analysis presented here is intrinsically approximate and preliminary. Only the simplest design information was developed during this project and no systems optimization was carried out for the storage concept. The primary conclusions which can be drawn from the cost data presented in Tables 7-11 depend on the relative contributions of components to the energy storage costs and present worth figures. These conclusions can be used as a guide for the next stage of design and engineering evaluation. For instance, the storage tank costs are a small part of the capital cost for storage times less than 6 hours. As a

result the other system components such as the droplet heat exchanger, the slag pumps and the connecting pipes tend to dominate the cost features of this storage concept for short storage times. However, the cost of higher storage times looks sufficiently attractive to warrant expanding the analysis of this concept to the total solar power system.

There are important systems considerations associated with the peak temperature of the storage system that are not directly accounted for in the present cost analysis. First, the power conversion apparatus can be smaller and possibly cheaper for a fixed power output, compared to a lower temperature, lower efficiency conversion system. The heat rejection apparatus for the power conversion subsystem is especially susceptible to economies from the use of a high temperature, high efficiency power cycle, since its size is proportional to $(\eta^{-1}-1)$ which magnifies the impact of larger efficiency. Secondly, the use of a high efficiency power cycle also reduces the size of the solar receiver and heliostat field, since less input power is required to produce the same output power. These offer substantial cost savings, compared to the cost of the storage system alone. The impact of high temperature operation, however, is often accompanied by increased material costs and the requirements for a high concentration ratio to achieve these temperatures will also place a burden on the optical quality of the heliostats, their alignment and on the positioning and design of the receiver, which will have potentially adverse cost impacts. It is too early to tell which influence will be the strongest. Yet the potential for substantial overall cost reductions suggests that this concept be further evaluated from a total power systems viewpoint.

5.0 CONCLUSIONS AND RECOMMENDATIONS

5.1. Conclusions

A very high temperature solar thermal energy storage system which uses molten slag as the storage medium and a droplet heat exchanger to extract the heat has been analyzed. Performance and cost data have been developed from a 10 MW_e point-design electric power system for 1, 6, 15 and 48 hours of storage and the costs have been compared to those of alternative storage concepts. Although the cost of the slag storage medium is very low in comparison with other storage media the overall storage system based on molten slag is more costly than other thermal storage technologies at all storage capacities considered. The major cost elements which result in this high cost are the slag-resistant α -alumina liners for the storage tank and pipes, the molten slag pumps and the droplet heat exchanger.

One important feature of the molten slag storage system is its ability to store and utilize heat at a much higher temperature than any other storage concept. This leads to smaller, higher efficiency power conversion apparatus and smaller heat rejection apparatus for a fixed power output, and to a reduction in the size of the solar receiver and heliostat field. These benefits may offer substantial cost savings, compared to the cost of the storage system alone.

High temperature process heat and fuels and chemicals production are applications for which the molten slag storage system may be particularly attractive. These applications require high temperatures which are beyond what current thermal storage technologies can provide and they represent large potential markets.

In conjunction with the cost and performance analysis a series of small-scale experiments with various slag compositions was undertaken with a view to study some of the properties of the slags and their compatibility with containment materials, and to explore the feasibility of droplet formation in a process similar to the method proposed for the droplet heat exchanger. The experiments encountered some difficulties at first but droplet formation in the range of 1-3 mm dia. was achieved.

5.2. Recommendations

Based on the results of the present study a number of recommendations can be made to improve the potential of the molten slag storage concept. First and foremost, a system optimization study and a cost sensitivity analysis should be carried out to develop a molten slag thermal storage system having the lowest possible cost. This evaluation should be from a total power systems viewpoint (i.e., including the heliostat, heat rejection apparatus, etc.). High cost, high leverage components such as the tank liner, droplet heat exchanger and slag pumps should receive particular attention. The slag-resistant tank and conduit liner is the most expensive component of the entire system and a search for lower cost alternative liner materials is essential to significantly reduce the system cost. Research is also needed to develop a lower cost slag pumping system, which at present represents more than one-half of the power-related costs. The droplet heat exchanger is less amenable to economies but here too a variety of cost-cutting measures are possible, such as a reduction in the quantity of molybdenum used in the droplet injector and the use of less expensive liners for the slag manifold and heat exchange chamber.

Also needed are additional small-scale experiments with molten slags to provide quantitative data on droplet formation. Experiments with small-scale droplet heat exchangers should also be carried out to determine the actual heat transfer rate from a multitude of droplets and to study the two-phase flow dynamics of the device. A more realistic and comprehensive model of the heating of the slag beads in the solar receiver is also required.

Finally the use of the molten slag storage system should be examined for applications requiring a very high temperature capability, such as thermochemical processing and high temperature process heat generation.

6.0. REFERENCES*

1. C. Wyman, "Thermal Energy Storage for Solar Applications: An Overview," SERI/TR-34-089, Solar Energy Research Institute, Golden, CO, 1979.
2. L.J. Dubberly, et. al, "Cost and Performance of Thermal Storage Concepts in Solar Thermal Systems,": Phase 1: SERI/TR-XP-0-9001-1-A, Phase 2: SERI/TR-XP-9001-1-B; Stearns-Roger Services, Inc., Denver, CO, 1981.
3. A. Hertzberg, "Overview of High Efficiency Power Cycles for Fusion, Proc. Intersociety Energy Conversion Engineering Conference, Seattle, WA, Aug. 18-22, 1980, pp. 1406-1411.
4. K. Cox, "Thermochemical Production of Hydrogen from Water: A Critical Review," Report No. LA-UR-78-2996, Los Alamos Scientific Laboratory, Los Alamos, NM, 1980.
5. J.F. Davidson and D. Harrison, eds., Fluidization, Academic Press, New York, 1971.
6. F.D. Richardson, Physical Chemistry of Melts in Metallurgy, Academic Press, New York, 1974.
7. "Engineering Property Data on Selected Ceramics: Volume III, Single Oxides," Report No. MC1C-HB-07-Vol. III, Metals and Ceramics Information Center, Battelle, Columbus Laboratories, Columbus, OH, 1981.
8. E.T. Turkdogan, Physical Chemistry of High Temperature Technology, Academic Press, New York, 1980.

*References cited in appendices are listed at the end of the corresponding appendix.

9. J.L. Bates, C.E. McNeilly and J.J. Rasmussen, "Properties of Molten Ceramics," in Materials Science Research, Vol. 5, W.W. Kriegel, ed., Plenum, New York, 1971.
10. W.D. Kingery, H.K. Bowen and D.R. Uhlman, Introduction to Ceramics, 2nd ed., John Wiley & Sons, New York, 1976.
11. J.F. Bacon, A.A. Hasapis and J.W. Wholley, Jr., "Viscosity and Density of Molten Silica and High Silica Content Glasses," Phys. and Chem. of Glasses 1, 90, 1960.
12. L. Shartsis, S. Spinner and W. Capps, "Density, Expansivity and Viscosity of Molten Alkali Silicates," J. Am. Ceram. Soc. 35, 155, 1952.
13. K.C. Lyon, "Prediction of the Viscosities of "Soda-Lime" Silica Glasses," J. Research NBS: A. Phys. & Chem. 78A, 497, 1974.
14. J.S. Machin and D.L. Hanna, "Viscosity Studies of System CaO-MgO-Al₂O₃-SiO₂: I, 40% SiO₂," J. Am. Ceram. Soc. 28, 310, 1945.
15. J.S. Machin, T.B. Yee and D.L. Hanna, "Viscosity Studies of System CaO-MgO-Al₂O₃-SiO₂: III, 35, 45, and 50% SiO₂," J. Am. Ceram. Soc. 35, 322, 1952.
16. J.S. Machin and T.B. Yee, "Viscosity Studies of System CaO-MgO-Al₂O₃-SiO₂: IV, 60 and 65% SiO₂," J. Am. Ceram. Soc. 37, 177, 1954.
17. E.T. Turkdogan and P.M. Bills, "A Critical Review of Viscosity of CaO-MgO-Al₂O₃-SiO₂ Melts," Ceramic Bull. 39, 682, 1960.
18. E.F. Osborn, R.C. De Vries, K.H. Gee and H.M. Kraner, "Optimum Composition of Blast Furnace Slag as Deduced from Liquidus Data for the Quaternary System CaO-MgO-Al₂O₃-SiO₂," Transactions AIME (J. Metals) 200, 33, 1954.

19. R.W. Wicker and E.F. Osborn, "Additional Phase Equilibrium Data for the System CaO-MgO-SiO_2 ," J. Amer. Cer. Soc. 37, 133, 1954.
20. A. Dietzel, "Praktische Bedeutung und Berechnung der Oberflächenspannung von Gläsern, Glasuren und Email," Sprechsaal (Deutschland), 75, 82, 1942. See also: "Beobachtungen an Chromroten Glasuren," Mitteilungsblatt der Deutschen Keramischen Gesellschaft (Deutschland), No. 1, pp. 12-14 and No. 2, pp. 15-21, 1949.
21. K.C. Lyon, "Calculation of the Surface Tensions of Glasses," J. Am. Ceram. Soc. 27, 186, 1944.
22. S.W. Freiman and L.L. Hench, "Further Analysis of Glass Crystallization Kinetics," J. Am. Ceram. Soc. 52, 111, 1969.
23. E.F. Foerster and P.L. Weston, Jr., "Heat Content of Some Blast-Furnace and Synthetic Slags," Report No. 6886, U.S. Department of the Interior, Bureau of Mines, 1967.
24. V.G. Voskoboinikov, "The Heat Capacity of Blast-Furnace Slags at High Temperatures," Teoriya i Prakt. Met. 12, 3, 1940 (in Russian).
25. E.A. Moelwyn-Hughes, Physical Chemistry, Pergamon Press, Oxford, 1964.
26. R.C. Weast, ed., Handbook of Chemistry and Physics, 52nd Ed., CRC Press, 1972.
27. J.H. Chesters, Refractories, The Iron and Steel Institute, London, 1973.
28. R.W. Brown, "Fused Cast Refractories," The Glass Industry, 45, 536, 1964.
29. L.M. Litz, "Graphite, Carbide, Nitride and Sulfide Refractories," Proc. International Symposium on High Temperature Technology, p. 90, Stanford Research Institute, 1959.

30. R. Manifold and W.E.C. Creyke, "Graphite as a Candidate Material for a Rotary Glass Fiberising Apparatus," Materials Sci. Engr. 33, 233, 1978.
31. E. Vago and C.E. Smith, "The Corrosion of Refractory Materials by Molten Glass," Proc. 7th International Congress on Glass, Technical Paper TP-848-I5, 1965.
32. C.B. Clark, "Petrology of the Reactions of Fused Cast Alumina Refractories with Metals and Slags," J. Metals 18, 1047, 1966.
33. R.W. Brown and K.H. Sandmeyer, "Fused Cast Refractories for the Chemical Process Industry," Preprint 32B, Symposium on Glass and Related Materials, Part II, Materials Conference, Philadelphia, PA, March 31-April 4, 1968.
34. W.A. Miller and W.L. Shott, "Corrosion of Refractories by Blast Furnace Slags," Am. Ceram. Soc. Bull. 47, 648, 1968.
35. J. Szekely, Fluid Flow Phenomena in Metals Processing, Academic Press, New York, 1979.
36. D.J. Hoteling, Penberthy Electromelt Int'l, Inc., Seattle, WA, private communication, 1981.
37. Detrick INTERSTOP Slide Gate Valves, M.H. Detrick Co., Chicago, IL.
38. R.H. Wilson, L.J. Conlon and W.P. Conrady, Research and Development on Advanced Graphite Materials, Vol. XXX, "Oxidation Resistant Graphite Base Composites," USAF Materials Laboratory, Report No. WADD TR 61-72, 1964.

APPENDIX A

SMALL-SCALE EXPERIMENTS WITH MOLTEN SLAGS

At the stage of this project when the task of formulating an appropriate composition for the thermal storage medium to be used in this system had just begun, it was decided to perform small-scale experiments with any potential compositions that might be of interest. Such experiments were not originally part of the work statement, but were deemed to be of sufficient importance to the program to be undertaken. The experimental facility would serve to model on a small scale some of the processes that would occur in an actual energy storage system of the type described in this report. The immediate applications for this facility were to 1) manufacture samples of the medium from the raw materials, 2) study its compatibility with containment materials, 3) study some of its physical and chemical properties, 4) acquire familiarity with high temperature working and testing techniques, and 5) eventually form droplets in a process similar to the method proposed for the droplet heat exchanger. In the following pages the facility and its use are described.

The thermal storage media chosen to be the best suited for the proposed application are glass-like slags composed of SiO_2 , CaO , MgO and Al_2O_3 , as noted in Section 2.0 of this report. Because of the relatively low silica content (40-50% by weight) of these slags, these materials have very low viscosities compared to common glass.

The compositions of interest can be obtained from a number of combinations of raw materials commonly used in ceramics production. Yellowstone talc, Sierralite talc, whiting and flint were chosen from among those raw materials readily available locally to yield slags with a minimum

of impurities. The percentage of impurities by weight in our slags total only ~1% by weight; these impurities consist primarily of metallic oxides which would necessarily be found as well in the materials used in any large scale thermal storage system of the kind currently under consideration. Further data on the raw materials are listed in Table A-1. The compositions of two slags that we have studied in our experiments to date are shown in Table A-2.

Once the raw materials powder has been mixed, it is heated in a suitable crucible using a 15 kW RF induction furnace. We have used cylindrical crucibles made of graphite and molybdenum with dimensions of 3 cm ID x 5 cm long and 0.5 cm thick wall. Graphite has excellent properties as a crucible material for our slag: it is very refractory, is not wetted by silica-based slags and is easily obtainable and easy to machine. Primarily

TABLE A-1
Compositions of the Raw Materials Used for Slag Manufacture

| | SiO ₂ | Al ₂ O ₃ | CaO | MgO | Other | LOI* |
|------------------|------------------|--------------------------------|------|-------|-------|-------|
| Yellowstone Talc | 62.0% | 0.2% | 0.2% | 32.0% | 1.25% | 10.6% |
| Sierralite Talc | 30.5 | 22.4 | 0.15 | 31.1 | 2.46 | 12.7 |
| Whiting | 1.0 | -- | 54.0 | 2.0 | 0.5 | 42.0 |
| Flint | 99.6 | 0.16 | 0.05 | 0.03 | 0.02 | 0.08 |

*LOI is weight percentage "Lost on Ignition" as a result of high temperatures driving off gases such as H₂O, CO₂, SO₂, or NO₂.

TABLE A-2
Slag Compositions and Batch Formulas (Weight Percent)

| | <u>SiO₂</u> | <u>Al₂O₃</u> | <u>CaO</u> | <u>MgO</u> | <u>Yellowstone Talc</u> | <u>Sierralite Talc</u> | <u>Whiting</u> | <u>Flint</u> |
|--------|------------------------|------------------------------------|------------|------------|-----------------------------|----------------------------|----------------|--------------|
| Slag A | 40%* | 5% | 35% | 20% | 36.66 | 21.64 | 63.75 | 9.55 |
| Slag B | 50% | -- | 30% | 20% | 58.84 | --- | 55.14 | 12.86 |

*Batch values may be up to .9% too high to account for 1.3% impurities in Slag A and 1.2% impurities in Slag B.

due to its easy machinability and availability, we have used it extensively for routine runs. However, for more elaborate experiments, molybdenum has proven to be more desirable because it suffers less corrosion than graphite under the conditions of our experiment, it is easier to control its contamination of the melt, and it is heated much more effectively in the RF induction oven. However, molybdenum is relatively expensive and difficult to machine. The induction furnace can heat either crucible material to the desired working temperature (>1650°K) within minutes, but as the powder fuses to form the slag, it releases gases such as H₂O and CO₂. Therefore the raw powder must be heated slowly to allow time for the degassing process to occur gradually.

Once a sufficient quantity of material has been produced from melting raw material powder in this way, it is permitted to solidify, is crushed, remelted and resolidified. This process is repeated twice to assure complete homogeneity of the slag melt for subsequent experiments. Free flow or vacuum draw droplet generation experiments can be performed with samples

of up to $\sim 11 \text{ cm}^3$ in volume. These experiments are done using crucibles having exchangeable nozzle inserts in the bottom. These inserts have various capillary diameters. The nozzles are 3-5 mm in length and the capillaries have diameters in the 1-4 mm range, with a rounded entrance. The molten sample flows through the capillary and falls into a cooling receptacle underneath the crucible.

The free-flow experiments depend on the pressure head of the slag inside the crucible to drive the materials through the nozzle. The method can be used to make a rough determination of the viscosity of the melt from a measurement of this flow rate through the nozzle capillary. This method of viscosity measurement is similar to that implemented in the well-known Saybolt viscosimeters. In our case, the method involves calibrating nozzles and crucibles with identical configurations at room temperature with oils and other high viscosity liquids.

The principal drawback of the free-flow experiment is that the melt is driven out under variable pressure--namely the dropping pressure head. For more determinate data, it was necessary to devise a method of achieving a constant and much higher driving pressure, so that the melt would stream through the nozzle at uniform velocity rather than merely seep through and drip.

Pressurization of the slag with a driving piston inside the crucible was briefly considered but rejected due to complications of non-uniform slag heating, piston freeze-up, etc. The technique finally selected (see Fig. A-1) involves pulling a vacuum beneath the crucible nozzle so that atmospheric pressure will drive the melt through the capillary. For the droplet formation experiments the crucible is supported by a high temperature graphite tube surrounded by a resistance heating element which

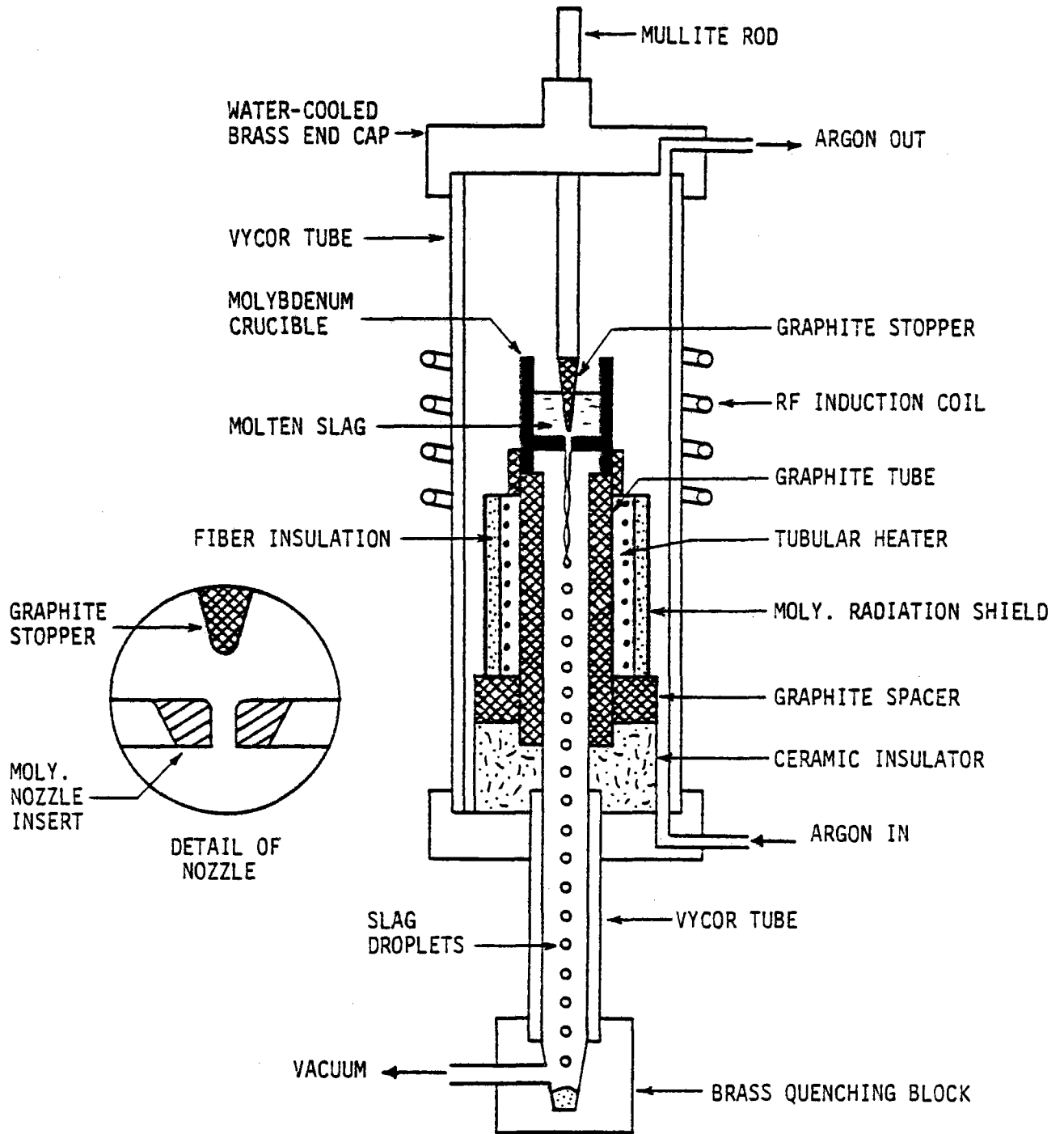


FIG. A-1 Schematic of experimental apparatus for molten slag droplet generation.

is in turn surrounded by a 1 cm layer of refractory fiber insulation and a molybdenum radiation shield. The heating element is a hollow ceramic cylinder, 23 cm in height, which serves to maintain a temperature of $\sim 1500^{\circ}\text{K}$ throughout the length of its interior. Thus, the stream of molten slag that exits from the nozzle of the crucible first passes through a high temperature zone and then drops about 50 cm down to a cooling receptacle. This hot zone immediately below the crucible greatly reduces the radiative cooling rate of the slag jet and permits the slag to retain its low viscosity long enough to be able to form spherical droplets before it reaches the relatively cold surroundings of the observation tube. The experimental facility (Fig. A-1) consists of two chambers: the upper and outer chamber contains the crucible and its supporting column housed in a 75 cm dia. vycor tube, and the lower, located directly beneath the crucible, is comprised of the heated graphite tube, a ceramic insulator section and a 25 mm dia. vycor tube which is closed off at the bottom by the brass quenching receptacle. A vacuum line is connected to this receptacle. The graphite and ceramic components of this lower chamber are cemented together with a high temperature ceramic adhesive (Sauresein Electrotemp, No. 8, rated at just over 1500°C).

After the upper chamber has been evacuated and subsequently purged with purified argon (which continues to flow through the upper chamber for the remainder of the experiment to inhibit oxidation of the molybdenum and graphite components), a graphite-tipped mullite rod is inserted through the top end cap. The graphite plug fits through a hole that has been molded into the powdered slag sample in the crucible. The plug is lowered to the bottom of the crucible to plug the capillary entrance.

The tubular ceramic heater is turned on and gradually brought up to 1500°K. The molybdenum crucible is heated by a ten-turn, 10 cm dia. x 13 cm long water-cooled induction coil surrounding the vycor tube and the enclosed crucible. The power on the induction unit (Inductotherm VIP Powertrack 15-96) is gradually increased to a value of around 7 kW for the interior of the molybdenum crucible to reach the test temperature of ~1700°K (determined with an optical pyrometer), melting the powdered slag within minutes. A vacuum pump is used to evacuate a 50 liter vacuum tank which is connected via a ball valve to the lower chamber of the heating facility. To start the slag flowing through the capillary nozzle, the vacuum ball valve is opened and the graphite plug is withdrawn from the crucible. Slag streams from the nozzle into the lower chamber, breaking up into droplets in the process. The droplets may be observed as they emerge from the bottom end cap of the large vycor tube and fall through the smaller vycor tube down to the brass quenching block. The brass quenching block acts as a heat sink for the falling droplets, which gather in a fused mass in the bottom of this receptacle.

Several droplet generation experiment runs have been performed with the system described above. The first two shakedown tests were a complete success; subsequent tests encountered a variety of difficulties, such as premature leakage of the slag, clogging of the nozzle and non-uniform melting. Due to the rapidity of the slag flow (~1-5 m/sec) conventional photographic techniques have not been adequate to record the self luminous slag droplets in flight. However, solidified droplets have been recovered, indicating that droplet formation does occur. A Dynafax high speed drum camera capable of 25,000 frames/sec has been obtained and will be used in future experiments. Backlit stroboscopic photographs are also planned.

Unfortunately, with the approximately five day recycle period for each of these runs (the facility must be completely disassembled and cleaned after each run), the experimental program could not be completed prior to the termination of this contract. However, at least it can now be demonstrated that small droplets of high temperature molten slag suitable for the heat storage system can indeed be produced by expulsion through small capillaries, as evidenced by the solidified slag droplets in the 1-3 mm size range collected during the two successful tests.

Furthermore, devising a pressurized system such as this one serves as a basis for future designs for larger scale systems. The technical difficulties involved in pumping a vacuum from a chamber at temperatures of up to 1750°K are in principle the same as maintaining a high pressure in the proposed droplet heat exchanger chamber. In conclusion, the experimental facility has supplied some useful practical experience with a specific thermal storage material composition and has clearly demonstrated the mechanical feasibility of generating molten slag droplets.

APPENDIX B

DROPLET GENERATION

Proper, highly effective operation of the droplet heat exchanger requires that droplets be neither carried out the top of the heat exchanger with the gas stream nor allowed to leave the bottom of the heat exchanger without having transferred most of their thermal energy to the gas stream. The rate of fall, heat capacity, heat transfer rate, and total transit time of droplets in the heat exchanger strongly depend on the droplet size. A relatively uniform droplet stream is essential for optimal droplet heat exchanger design and operation.

A small stream of a liquid with moderate viscosity and surface tension will break up shortly after emerging from an orifice due to the pinching action of surface tension. The actual breakup process is governed by the growth of surface instabilities on the liquid stream and results in a relatively broad distribution of droplet sizes. As described below, the jet instability can be utilized to provide a multitude of uniformly sized droplet streams at the top of a droplet heat exchanger by suitably exciting the jet. Although the theory of liquid jet breakup is well developed and amply verified by experiments with familiar low viscosity, low surface tension fluids, some uncertainty exists regarding the high viscosity, high surface tension slags which we have proposed. Additional factors such as high liquid jet cooling rates and resulting rapid viscosity changes of such high temperature liquids could significantly affect the breakup of the liquid jet. Required extensions to the existing analytical and data base for droplet formation processes will be discussed after the current status of this technology is reviewed.

The breakup of inviscid liquid jets was first studied by Rayleigh.^{1*} The effects of viscosity and aerodynamic forces were included in an analysis by Weber.² A number of more recent studies³⁻⁶ have shown that the breakup can be facilitated by subjecting the stream to a mechanical vibration.

A single jet emerging into the heat exchanger at uniform velocity is shown in Fig. B-1. The breakup is described in terms of the deviation of a streamline from its original location. For the outer surface of the stream, the deviation λ is given as a function of time, t , by

$$\lambda = \lambda_0 e^{\eta t} \quad (B-1)$$

where λ_0 is an initial disturbance and η is the amplification factor which is a function of the wave parameter α , given by

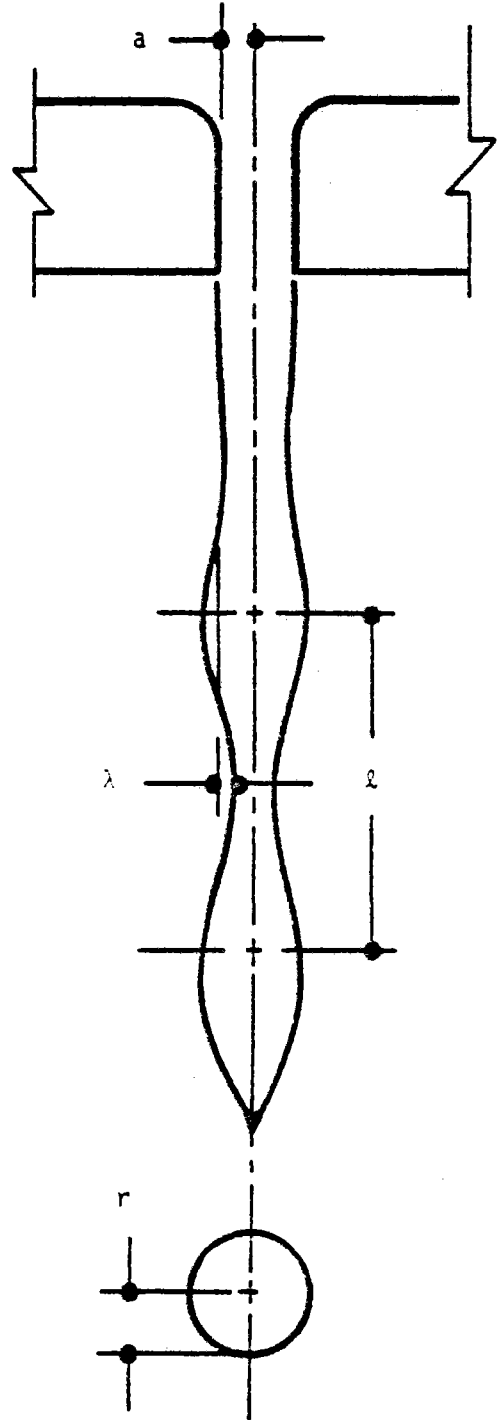
$$\alpha = 2\pi a / \ell \quad , \quad (B-2)$$

where a is the initial jet radius and ℓ is the wavelength of the disturbance. The analysis of Wickemeyer⁵ for a viscous, constant velocity stream with aerodynamic forces results in $\eta(\alpha)$ being given as

$$\eta^2 + \left(\frac{3\mu}{\rho a^2}\right) \alpha^2 \eta = \frac{\sigma}{2\rho a^3} (1-\alpha^2) \alpha^2 + \frac{\rho_g}{2\rho a^2} U_r^2 \alpha^3 \frac{K_0(\alpha)}{K_1(\alpha)} \quad (B-3)$$

where the density ρ , viscosity μ , and surface tension σ are for the emerging jet. The density of the gas is ρ_g and U_r is the relative velocity between

*References are listed at the end of the Appendix.



- $\alpha = 0.36$
- $\eta = 353 \text{ Hz}$
- $a = 0.21 \text{ mm}$
- $r = 0.5 \text{ mm}$
- $\ell = 3.7 \text{ mm}$
- $f = 390 \text{ Hz}$

Fig. B-1 Geometry of Jet Breakup.

the jet and the gas. K_0 and K_1 are the modified Hankel functions of order zero and one, respectively.

For a given set of parameters η reaches a maximum value η_{\max} , at a particular value of the wave parameter, α_{\max} . It can be shown that in the absence of external influences the jet breaks up uniformly at coordinates corresponding to the maximum value of η , i.e., at

$$\frac{\partial \eta}{\partial \alpha} = 0 \quad (\text{B-4})$$

Thus, an initial random disturbance grows at the fastest possible rate:

$$\lambda = \lambda_0 e^{\eta_{\max} t} \quad (\text{B-5})$$

The stream breaks up when the magnitude of the disturbance attains the radius of the stream, i.e., when $\lambda = a$. The breakup time follows from Eq. (B-5):

$$t_{\text{bu}} = \frac{1}{\eta_{\max}} \ln \left(\frac{a}{\lambda_0} \right) \quad (\text{B-6})$$

The breakup distance, x_{bu} , is related to the breakup time and the average velocity of the jet, U_j , by

$$x_{\text{bu}} = t_{\text{bu}} U_j \quad (\text{B-7})$$

and the rate of drop generation is given by

$$f = U_j / \ell \quad (\text{B-8})$$

The size of the drop can be determined from the equation of continuity:

$$\frac{4}{3} \pi r^3 = \pi a^2 l \quad , \quad (B-9)$$

where r is the drop radius. Thus,

$$r = a \left(\frac{3}{2} \frac{\pi}{\alpha_{\max}} \right)^{1/3} . \quad (B-10)$$

By subjecting the stream to mechanical vibration, the breakup of the jet can be greatly facilitated. The frequency of drop generation, the size of the drops, and the breakup distance can be varied over a range which corresponds to a range of α in the vicinity of α_{\max} . In other words, by means of external excitation the stream can be forced to break up at values of η different from η_{\max} . This is a result of $\eta(\alpha)$ having a relatively broad maximum, so that an externally applied cyclic disturbance of sufficient amplitude can grow at the expense of the natural vibrational mode. Since natural disturbances tend to be random, external excitation greatly improves the stability of the breakup process.

Figure B-1 displays the parameters predicted for the formation of slag droplets of 1 mm diameter at 1650°K ($\mu = 7$ poise, $\sigma = 420$ dyne/cm) and 1.44 m/sec injection velocity. These conditions correspond to those which exist in the droplet heat exchanger considered in Appendix C. The excitation frequency of 390 Hz could be supplied by direct mechanical vibration of the injector nozzle plate or by cyclic pulsation of the injection pressure.

Deviations from Simple Model

Due to the fact that the surface tension and viscosity of the glassy slag of interest for the high temperature thermal storage system are much higher than values for which the analytical model discussed above has been verified, some uncertainty exists in the accuracy of droplet sizes, breakup distance, and optimal excitation frequency for molten slags. Since the growth of surface instabilities is damped by the fluid viscosity, suppressing droplet formation, and is enhanced by surface tension, significant differences between projected and actual droplet formation parameters may occur when these properties vary by orders of magnitude. The latter has particular relevance to the droplet heat exchanger because of the initially rapid cooling that the stream may undergo as a result of both radiative and convective heat transfer. This cooling would result in an increase in viscosity along the length of the emerging jet, which would delay the breakup process. Another factor which needs to be considered is the gravitational acceleration of the jet prior to breakup. This causes the jet to neck down⁶ and alters the geometrical parameters of the simple model.

Recent experimental work with viscous oils (up to 15 poise) indicates that although the droplet formation process does indeed appear to deviate from that predicted by the simple linear theory discussed above, its main features remain the same, i.e., droplet sizes, separation distances, and breakup length are greater than predicted by the linear theory but stable and uniform droplet generation is still possible within useful ranges of the jet flow parameters.⁷

References - Appendix B

1. Rayleigh, J.W.S., "On the Instability of Jets," Proc. London Math. Soc. 10, 4 (1878).
2. Weber, C., "Zum Zerfall eines Flursigkeitsstrahiles," Z. Agnew Math. Mech. 11, 136 (1931).
3. Crane, L., Birch, S. and McCormack, P.D., "The Effect of Mechanical Vibration on the Break-Up of a Cylindrical Water Jet in Air," Brit. J. Appl. Phys. 15, 743 (1964).
4. McCormack, P.D., Crane, L. and Birch, S., "An Experimental and Theoretical Analysis of Cylindrical Liquid Jets Subject to Vibration," Brit. J. Appl. Phys. 16, 395 (1965).
5. Wickemeyer, R.H. and Oppenheim, A.K., "Breakdown of a Liquid Filament into Drops Under the Action of Acoustic Disturbances," Technical Note No. 1-67, Report No. AS-67-6, University of California Office of Research Services, Berkeley, CA (1967).
6. J.N. Anno, The Mechanics of Liquid Jets, D.C. Heath & Co., Lexington, MA, 1977.
7. W.J. Thayer, Mathematical Sciences Northwest, Inc., Bellevue, WA, private communication, Aug. 1982.

APPENDIX C

THE DROPLET HEAT EXCHANGER

The accessibility of the stored energy to the working fluid of the energy conversion system has proved to be a problem in many of the energy storage systems considered to date. Typically, some form of conventional tube-type heat exchanger is used to transfer heat between the storage and working media. Such devices involve heat transfer through surfaces and are consequently temperature limited by materials considerations. Tube-type heat exchangers also impose significant pressure drops, tend to be complex and are susceptible to single point failure and fouling.

The thermal energy storage system described here allows direct contact of the storage material with the working gas at high temperature in a droplet heat exchanger, circumventing many of the classical limitations of conventional heat exchangers. The droplet heat exchanger consists of a single, large, insulated cylindrical pressure vessel. One possible conceptual configuration is illustrated in Fig. 8, in Section 3.7. A pressurized gas pumping system (see Section (3.6) is used to force molten slag from the slag storage tank through an insulated refractory pipe. The molten slag is injected into the heat exchanger through a suitable refractory metal nozzle plate pierced with a multitude of small holes. The resulting liquid streams can be made to break up into a series of uniform drops by pulsing the feed pressure at the appropriate frequency (see Appendix B). The droplets fall through the heat exchanger, giving up their heat to an inert working gas (such as argon or nitrogen) by convective, conductive and radiative processes. The heated gas is then used as the working fluid in a high temperature heat engine.

Heat Transfer Analysis

Once a uniform distribution of droplets is generated at the top of the heat exchanger column, a number of coupled gas and droplet flow and heat transfer processes occur simultaneously and control the performance of this type of device. For the purpose of the present analysis we have developed a simple one-dimensional two-phase flow model of the heat exchanger based on the geometry of Fig. C-1. The constitutive equations for this model are summarized below, followed by a presentation of numerical solutions for gas and droplet velocity and temperature profiles and heat exchanger configuration for a baseline design. The approach is based on the work of Marble¹ and Rudinger.²

The heat exchanger is assumed to be a vertical cylindrical chamber with an adiabatic side wall. The droplets are all injected axially downwards at their terminal velocity with respect to the gas at the conditions existing at the top of the chamber. The droplets are of uniform diameter and are uniformly distributed across the flow area. The counterflowing gas is assumed to have a uniform radial velocity profile.

The continuity equations for the gas and droplets, for steady, constant area flow are:

$$(1-\beta)\rho u = \text{const} \quad (\text{C-1})$$

$$\beta\rho_p u_p = \text{const} \quad (\text{C-2})$$

where ρ and u are the gas density and velocity, ρ_p and u_p are the droplet material density and velocity, and β is the volume fraction occupied by the droplets. (Velocities are considered positive in the direction of droplet motion, i.e., downward).

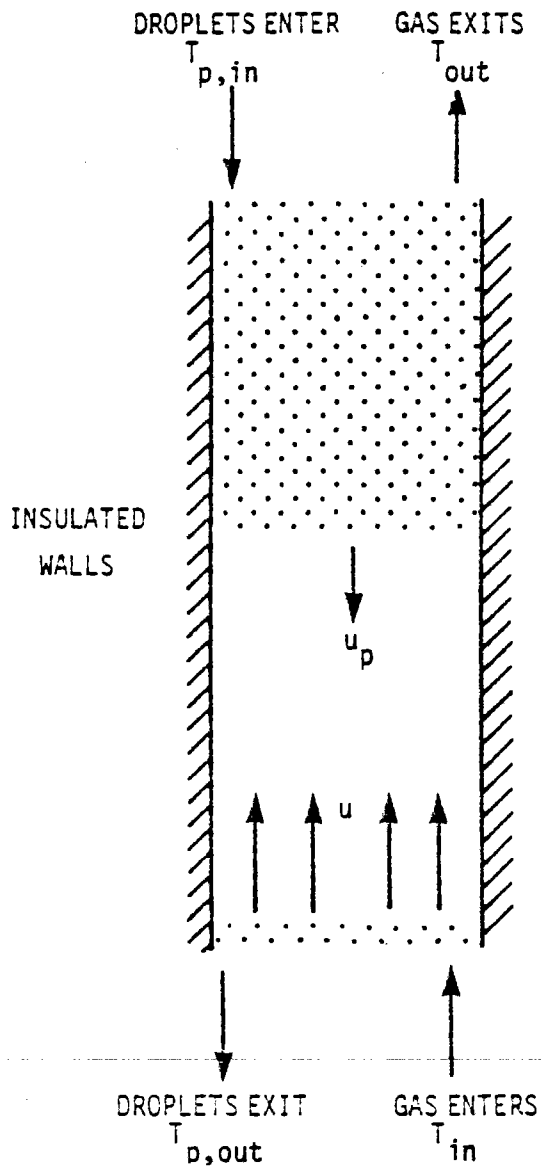


Fig. C-1 Schematic of 1-D droplet heat exchanger model.

The ratio of mass flow rates of the droplets and gas can be chosen arbitrarily, though usually such as to maximize heat exchanger effectiveness or to tailor the temperature profile. In most cases it is expected that this ratio will be in the vicinity of the inverse specific heat ratio, i.e., the case of matched thermal flow capacities. Thus

$$(1-\beta)\rho u C_p \approx \beta \rho_p u_p C_s \quad (C-3)$$

where C_p and C_s are the specific heats at constant pressure of the gas and droplets, respectively.

In the case of slag droplets ($\rho_p = 2.9 \text{ g/cm}^3$, $C_s = 0.3 \text{ cal/gm/}^\circ\text{K}$) falling through argon at 20 atm and 1500°K ($\rho = 6.5 \times 10^{-3} \text{ g/cm}^3$, $C_p = 0.124 \text{ cal/gm/}^\circ\text{K}$) at velocities comparable to the gas velocities, we find $\beta \approx 10^{-3}$ and thus $1-\beta \approx 1$. This result is applicable over a wide range of pressures, temperatures and velocities.

The momentum equations for the gas and droplet phases are respectively:

$$\rho u \frac{du}{dx} = - \frac{dp}{dx} - \frac{3}{4} \frac{\beta \rho C_D (u_p - u) u_p - u}{d} \quad (C-4)$$

$$\rho_p u_p \frac{du_p}{dx} = \rho_p g - \frac{3}{4} \frac{\rho C_D (u_p - u) u_p - u}{d} \quad (C-5)$$

where x is axial the distance of the droplet from the plane of the injector, d is the droplet diameter, p is the gas pressure, C_D is the drag coefficient and g is the acceleration of gravity. For this analysis the single particle correlation for C_D for $Re < 1000$ given by Klyachko³ was used:

$$C_D = \frac{24}{Re} + \frac{4}{Re^{1/3}} \quad (C-6)$$

where $Re = \rho u_p d / \mu$ is the droplet Reynolds number and μ is the gas viscosity. For $1000 < Re < 10^5$, we have assumed $C_D = 0.42$. These correlations for C_D are applicable when the volume fraction of droplets is small.

The convective heat transfer between the droplets and the gas is governed by the Nusselt number, $Nu = hd/k$, where h is the heat transfer coefficient and k is the thermal conductivity of the gas. Due to the lack of consistent Nusselt number data for heat transfer between a cloud of particles and a gas we have assumed the single particle correlation of Rowe, et al.⁴

$$Nu = 2 + 0.74 Pr^{1/3} Re^{1/2} \quad , \quad (C-7)$$

where $Pr = C_p \mu / k$ is the Prandtl number of the gas.

The thermal conductivity of the glassy slag proposed as the thermal storage medium is much higher than the thermal conductivity of the any working gas of interest. For slag droplets of the order of 1 mm in diameter and most gases except hydrogen, it can be shown that the Biot number,⁵ $Bi = hd/6k_s < 0.2$ (where k_s is the thermal conductivity of the droplet medium) and thus it can be assumed that the interiors of the droplets are at a uniform temperature.

Accordingly, the equations governing the temperatures of the falling droplets and the counterflowing gas are respectively:

$$\rho_p u_p \frac{dT_p}{dx} = - \frac{6N_u k}{C_s d^2} (T_p - T) - \phi[T, T_p, f(T_w)] \quad (C-8)$$

$$\rho u \frac{dT}{dx} = \frac{6N_u k}{C_p d^2} \beta (T_p - T) + \theta[T, T_p, f(T_w)] \quad (C-9)$$

where T_p is the droplet temperature, T is the gas temperature, ϕ and θ are the radiative interaction terms and $f(T_w)$ is the chamber wall temperature distribution.

ϕ and θ are functions of the optical properties of the gas and the cloud of particles at the conditions existing in the heat exchanger, the dimensions of the heat exchanger and the temperature distribution of the cavity walls, as well as the droplet and gas temperatures. In general, the determination of the radiative interaction terms is very difficult.⁶ Under a related DOE contract,⁷ we are currently formulating the details of the radiative transport phenomena in the heat exchanger, including emission, absorption and scattering by the particles, emission and absorption by the gas and reradiation by the side walls of the container. For our present purposes it suffices to summarize two limiting cases, which consist of the optically thin and optically thick approximations.

Optically Thin Approximation - If the mean-free-path of radiation in the gas-particle mixture is of the order of or larger than the characteristic dimensions of the heat exchanger column there is no gas radiative interaction term and no particle-to-particle interaction term. The particles interact radiatively only with the walls. We have used the zone method of Hottel⁸ to determine the temperature distribution of the

reradiating adiabatic side walls (assumed to be black). The side wall was divided into 10 zones and radiative view factors between the particles and the individual zones, and upper and lower ends, were computed as a function of particle position by the technique of Feingold and Gupta.⁹ The dimensions of the heat exchanger and the temperature of the bottom end must be known a priori and consequently the solution must proceed iteratively. (The temperatures of the upper and lower ends are assumed equal to the inlet and outlet droplet temperatures, respectively). A first solution is obtained without the radiative term to generate first approximations. Subsequent iterations include the radiative term and are carried out until convergence is achieved. Usually, three iterations are sufficient for convergence within 1% of column height.

Optically Thick Approximation - This case is of interest for large heat exchanger cavities in which the droplet cloud is optically thick. The optical thickness or optical mean free path of the cloud of particles is given by ⁶

$$\lambda_{\sigma} = \frac{1}{n\sigma_t} \quad (C-10)$$

where n is the particle number density and σ_t is the sum of the microscopic absorption and scattering cross-sections, σ_a and σ_s , respectively. We can determine n from

$$n = \frac{\beta}{V_p} \quad (C-11)$$

where $V_p = 4/3\pi r^3$ is the volume of a single particle. For particles whose diameter is much larger than the wavelength of light, as is the case here, σ_s is approximately equal to twice the geometrical cross section.⁶ The absorption cross-section σ_a depends on the spectral absorption characteristics of the particle material, but for present purposes will be approximated by its geometrical cross section. Consequently, σ_t is approximately equal to three times the geometrical cross-section. Accordingly,

$$\lambda_\sigma \approx \frac{2d}{9\beta} \quad . \quad (C-12)$$

For $\beta \approx 10^{-3}$ and $d = 1 \text{ mm}$, $\lambda_\sigma \approx 0.25 \text{ m}$. Thus, if the dimensions of the cavity are considerably larger than λ_σ , we can consider the cloud of particles to be optically thick. For such a case it has been shown that radiative heat transfer in the axial direction is small compared to the convective heat transfer, due to self-trapping.¹ In the radial direction the radiative transfer acts as an enhanced effective conductivity which can be much greater than the gas conductivity. However, if the walls are adiabatic, they will tend to attain an axial temperature profile similar to that of the particles, with the result that the particle temperature profile will, in the steady state, be approximately the same as if there were no radiative heat transfer at all. As will be shown later, the dimensions of a droplet heat exchanger which transfers 23 MW_{th} under the conditions prescribed by the present system place it in the optically thick category.

Baseline Design Calculations

We present here the results of numerical calculations for heating argon at 20 atm by molten slag droplets (50% SiO₂, 30% CaO, 20% MgO) injected into the heat exchanger at 1650°K. Argon inlet and exit temperatures of 862°K and 1500°K were respectively chosen for our baseline system to match a high temperature regenerative Brayton cycle. The Brayton cycle was assumed to operate with a turbine inlet temperature of 1500°K at 20 atm and a turbine pressure ratio of 5. For compressor and turbine efficiencies of 0.85 and 0.88, respectively, and a recuperator effectiveness of 0.95 the cycle efficiency is 43%. Assuming no electric generation losses, a pilot solar thermal plant of 10 MW_e output would require 23 MW of thermal power to be delivered to the turbine inlet. The heat exchanger was sized accordingly. The mass flow rates of the two media were adjusted to match their thermal flow capacities, although any suitable mass flow ratio may be chosen to tailor the temperature profiles or heat exchanger effectiveness to specific needs. For the matched heat capacity case this power level requires a mass flow of slag of 1.0×10^5 kg/hr and a mass flow of argon of 2.5×10^5 kg/hr.

Tabulated data¹⁰ for the viscosity, thermal conductivity and specific heat of argon, as functions of temperature at the given pressures, were subjected to a fourth-order curve fitting procedure to obtain analytical expressions for use in the analysis. The ideal gas law was used for the equation of state of argon. The variation of the heat capacity of the slag mixture as a function of temperature was approximated by the correlation discussed in Section 2.4.

As noted earlier, the droplets are injected at their terminal velocity with respect to the gas at the conditions existing at the top of the heat exchanger. The gas velocity at the top is a free parameter but for the

present baseline analysis has been chosen to be 50% of the droplet terminal velocity. Thus the droplets' injection velocity with respect to the heat exchanger is also 50% of terminal. This choice of droplet injection velocity and gas velocity results in a compromise among heat exchanger height, diameter and number of slag injection orifices.

For a given working gas at a given pressure the size of the heat exchanger is strongly dependent on the particle size and on the choice of droplet injection velocity and gas outlet velocity. For example, decreasing the droplet size reduces the height. Reductions in height also result if the droplet injection velocity is reduced or if the gas outlet velocity is increased. Reducing the droplet size or injection velocity, however, increases the required number of droplet injection orifices. Increasing the gas velocity reduces the diameter of the heat exchanger, as well as its height, without affecting the number of slag injection orifices but can lead to entrainment and lofting of the droplets. Droplets of 1 mm diameter and the aforementioned choice of droplet and gas velocities at the top of the device appear to provide a reasonable compromise for present purposes, resulting in a heat exchanger column 6.5 m high and 3.0 m diameter, under the optically thick assumption. It is now evident that this assumption was valid, since the dimensions of the column are much greater than the optical mean free path of 0.25 m calculated earlier.

The velocity profiles of the droplets and argon for this case are shown in Fig. C-2. The droplets traverse the heat exchanger in 4.9 sec. The gas velocity is so low throughout the heat exchanger that its momentum and kinetic energy are negligible. The droplet volume fraction, β , varies from 9×10^{-4} at the top of the heat exchanger column to 7.6×10^{-4} at the bottom and gives rise to a negligible total static pressure head. The total pressure

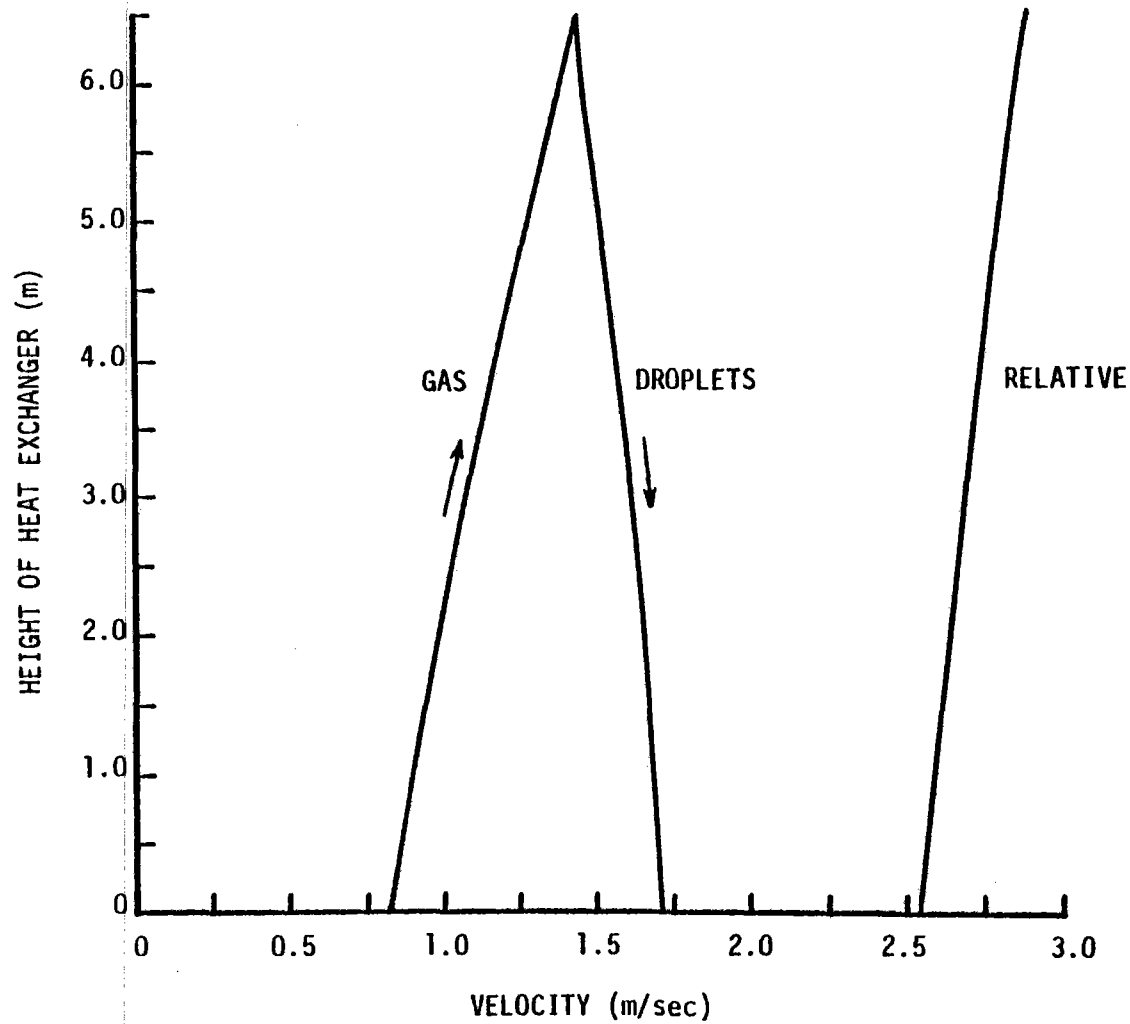


Fig. C-2 Axial velocity profiles in droplet heat exchanger for heating argon at 20 atm. Droplet dia. = 1.0 mm.

drop of the argon between the bottom and top of the heat exchanger is 7×10^{-3} atm, or less than 0.04% of the inlet gas pressure.

The axial temperature profiles of the slag droplets and working gas for the case considered are shown in Fig. C-3. These correspond to the optically thick assumption. The effectiveness of this particular droplet heat exchanger is 0.85.

It is interesting to compare the results based on the optically thin assumption with the results for the optically thick case presented above. Figure C-4 shows the temperature profiles of the particles and argon for the same parameters as used in Figure C-3 and a droplet emissivity of 0.5. Also shown here is the side wall temperature distribution as calculated by Hottel's zone method.⁸ The effect of the radiative interaction is to increase the temperature difference between the droplets and the gas towards the bottom of the heat exchanger. This result follows from the higher temperature of the side wall as compared to that of the particles for much of the height of the column. Note also that the height of the heat exchanger is reduced; this is a result of enhanced heat transfer due to the increasing temperature difference between the two media. The heat exchanger effectiveness, however, is considerably degraded by what effectively is a short-circuiting of the device by the radiative transfer. For the present case the effectiveness is reduced from 85% to 71%. It should be emphasized that the optically thin approximation outlined above is not applicable to droplet heat exchangers of the scale considered here, but is useful in illustrating the "worst case" effects of radiative transfer.

Although the droplets solidify during their transit down the heat exchange column, the release of heat of fusion is negligible due to the slow crystallization rate of the slag droplet material, as noted in Section 2.4,

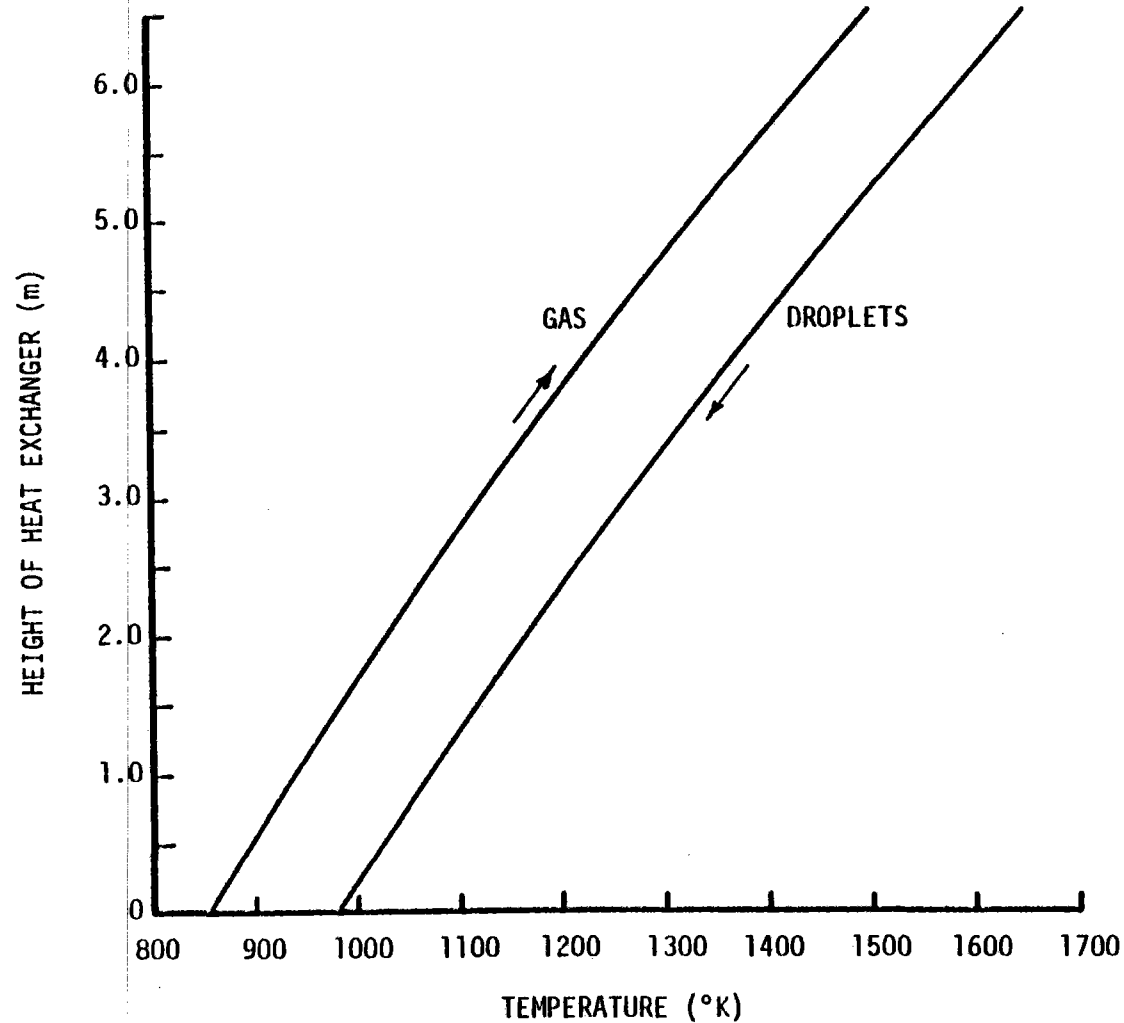


Fig. C-3 Axial temperature profiles in droplet heat exchanger for heating argon at 20 atm. Droplet dia. = 1.0 mm. Optically thick approximation.

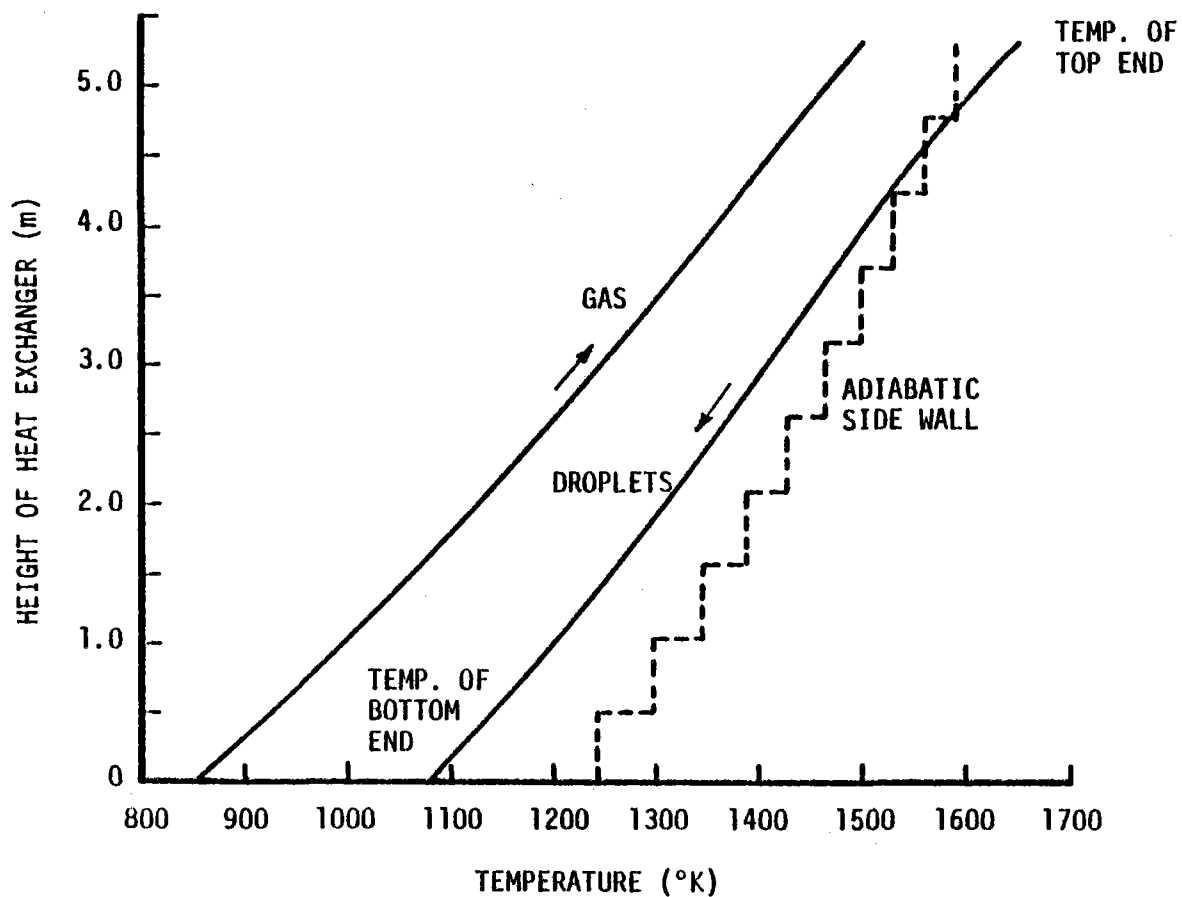


Fig. C-4 Axial temperature profiles in droplet heat exchanger for heating argon at 20 atm. Droplet dia. = 1.0 mm. Optically thin approximation; emissivity of droplet = 0.5. Adiabatic black-body sidewall temperature computed by Hottel's zone method.

and thus has not been included in the present analysis. Any suitable temperature difference between the droplets and the gas at the top of the heat exchanger may be chosen. Higher temperature differences reduce the height of the column but decrease the effectiveness.

The interaction of the flow with the walls, turbulence, end effects and other flow non-uniformities will cause deviations from the simple one-dimensional flow assumed in the foregoing calculations. Collisions between droplets in the area of the heat exchanger where they are still molten may result in some degree of agglomeration of the individual droplets which will affect both the heat transfer rate and the velocity relative to the gas. Droplets near the periphery of the heat exchanger cavity may collide with the walls and either bounce off, form a liquid film or bead up, depending on whether they are still molten, on the collision energy and on whether the wall is wetting or non-wetting. Slag adhering to the wall could build up an undesirable cake as it runs down towards lower temperature regions where it would solidify. These problems, together with the design of the liquid, solids and gas manifolds are the subject of ongoing theoretical and experimental investigations by the authors and their colleagues.⁷

References - Appendix C

1. F. Marble, "Dynamics of a Gas Containing Small Solid Particles," Combustion and Propulsion, 5th AGARD Colloquium, MacMillan & Co., New York, 1963.
2. G. Rudinger, "Relaxation in Gas-Particle Flow," Nonequilibrium Flows, Part I, Marcel Dekker, New York, 1969.
3. N.A. Fuchs, The Mechanics of Aerosols, MacMillan & Co., New York, 1964, p. 33.
4. P.N. Rowe and K.T. Claxton, Trans. Inst. Chem. Eng. (London) 43, 321, 1965.
5. F. Kreith, Principles of Heat Transfer, International Textbook Co., Scranton, PA, 1958.
6. R. Siegel and J.R. Howell, Thermal Radiation Heat Transfer, 2nd ed., McGraw Hill, New York, 1981, pp. 412-489.
7. W.J. Thayer, et al., "Development of Droplet Heat Exchangers," DOE Contract AC06-81-ER10918, Mathematical Sciences Northwest, Bellevue, WA.
8. H.C. Hottel, "Effect of Reradiation on Heat Transmission in Furnaces and Through Openings," Trans. ASME 55, 39, 1933.
9. A. Feingold and K.G. Gupta, "New Analytical Approach to the Evaluation of Configuration Factors in Radiation from Spheres and Infinitely Long Cylinders," J. Heat Transfer 92, 72, 1970.
10. N.B. Vargaftik, Tables of the Thermophysical Properties of Liquids and Gases, John Wiley & Sons, 1963.

APPENDIX D

CONTAMINATION OF THE WORKING GAS BY SLAG VAPOR

The contamination of the working gas by vaporization of the slag droplets can be easily estimated. Since the decrease of vapor pressure with decreasing temperature is very steep for the slag (and, indeed, for all materials), most of the evaporation occurs at the hot, or upper, end of the droplet heat exchanger. Assuming that the working gas leaving the heat exchanger is saturated with slag vapor (see Section 2.6) at the partial pressures corresponding to the highest droplet temperature (1650°K*), the volume flow rates of vapor and working gas will be in the same ratio as their respective partial pressures, P_v and P_g . Assuming ideal gas behavior, it follows that the mass flow rate of vapor is given by:

$$\dot{m}_v = \frac{\dot{m}_g P_v T_g M_v}{P_g T_v M_g}$$

where \dot{m}_v and \dot{m}_g are the mass flow rates of slag vapor and working gas, respectively, and T_v and T_g , and M_v and M_g are the temperatures and molecular weights of the two species.

In Section 2.6 it was noted that slag vapor actually consists of SiO and O₂. At 1650°K the respective partial pressures of these species are:

*The working gas will actually be supersaturated with slag vapor because the gas temperature is 150°K colder than the droplet temperature.

$$p_{\text{SiO}} = 3.45 \times 10^{-8} \text{ atm}$$

$$p_{\text{O}_2} = 1.78 \times 10^{-8} \text{ atm} .$$

Also, $T_g = 1500^\circ\text{K}$, $T_v = 1650^\circ\text{K}$, $\dot{m}_g = 2.5 \times 10^5 \text{ kg/hr}$, $M_g = 40$, $M_{\text{SiO}} = 44$ and $M_{\text{O}_2} = 32$. Thus, we obtain

$$\dot{m}_{\text{SiO}} = 4.3 \times 10^{-4} \text{ kg/hr}$$

$$\dot{m}_{\text{O}_2} = 1.57 \times 10^{-4} \text{ kg/hr}$$

which is equivalent to a contamination of 1.7 ppb of SiO and 0.6 ppb of O₂, both very small amounts.

Of these two contaminants, SiO is potentially the more troublesome because it condenses out as a solid in the form of particulates in the colder components of the system. However, this condensation would be as a very dilute suspension of submicron particles most of which would remain entrained in the gas flow. The precipitation of SiO on colder engine parts is not expected to be important in this system. Recently, Sims et al.¹ reported on a series of experiments in which they measured the deposition of sodium salts (chloride and sulfate) on hot stage hardware in a gas turbine at various loadings. In one particular test the sodium loading was 30 ppb, gas temperature 1340°K and turbine blade temperature 1255°K. After 60 hours they measured a sodium sulfate deposition of 0.1 mg over a 10 cm² area (equivalent to a coating only ~0.04 μm thick). In our case the concentration of SiO in the output of the droplet heat exchanger is nearly a factor of 20 lower than the case studied by Sims et al. Thus, for our system it would take ~1200 hours to accumulate the same amount of

precipitate on the blades. It is clear that the turbine would be able to operate for many thousands of hours without requiring any removal of the contaminant vapors from the working gas.

References - Appendix D

1. C.T. Sims, H. von E. Doering and D.P. Smith, "Effects of the Combustion Products of Coal Derived Fuels on Gas Turbine Hot Stage Hardware," Paper No. 79-GT-160, ASME Gas Turbine Conference, San Diego, CA, March 12-15, 1979.

APPENDIX E

INJECTION AND TRANSPORT LOSSES

The injection pressure drop can be determined from a knowledge of the stream geometry, velocity and the viscosity of the fluid. For a nozzle diameter of 0.4 mm and length of 2.5 mm, the required pressure drop across the injector for slag injection at 1650°K is 5 atm, assuming Poiseuille flow and including entrance effects.¹ Adding to this the 20 atm static pressure of the working gas in the heat exchanger the 10 MW_e plant used as our example will require 24 kW to pressurize and inject the slag at the required rate of 27.8 kg/sec.

The transport losses in the piping which connects the storage reservoir to the heat exchanger can be calculated in a similar way. Assuming a pipe diameter of 25 cm, which results in an average flow velocity of 0.2 m/sec, and a total pipe length of 20 m, the power loss necessary to overcome viscous losses is only 14 W, assuming laminar flow. The hydrostatic losses incurred in raising the slag to the top of the heat exchanger (assumed to be ~7.5 m above pump level) require an additional expenditure of ~2.5 kW. Thus, the total parasitic losses due to injection and transport of the molten slag in the baseline system presented here add up to 26 kW or less than 0.3% of the plant's net electrical output. To this figure must be added the power required to handle the solid aggregate and to provide normal stationkeeping functions. It is expected that the total circulating power fraction necessary for all these tasks will not significantly exceed typical values characteristic of conventional fuel-fired central power systems.

References - Appendix E

1. L. Prandtl and O.G. Tietjens, Applied Hydro- and Aeromechanics, Dover Publications, New York, 1934.

APPENDIX F

WORKING GAS LOSSES

The solidified refractory beads must be removed from the bottom of the heat exchanger without allowing loss of pressure from the heat exchanger vessel. One concept for accomplishing this is the rotary valve shown in Fig. F-1. The solid beads enter the valve at the top and are carried around to the bottom by the rotating vanes. The vanes are arranged so that there is always at least one vane touching the housing on each side to maintain a pressure seal.

Since the beads, even when closely packed, do not fill the valve volume completely, some of the working gas will be carried out in the interstitial volume of the bead aggregate. Assuming the beads are spherical, and closely packed, the interstitial volume will be 28% of the volume occupied the beads. For the heat exchanger presented above, using slag with a density of 2.9 g/cm^3 and argon at 20 atm and 980°K , 133 kg/hr of argon would be carried out with the beads, or about 0.04% of the mass flow of argon. By first passing the exiting aggregate through a degassing chamber kept at 0.1 atm, and then through a second rotary valve, most of the lost argon can be recovered. The loss rate can be reduced by a factor of 200 in this manner to about 0.67 kg/hr (2.7×10^{-6} of the total mass flow of argon through the system). The yearly consumption of argon, assuming an 80% duty cycle, would then be ~4700 kg/yr. If other gases such as nitrogen or carbon dioxide were used the loss rates would be of a similar order of magnitude. The cost of these gases is, of course, much lower than the cost of argon and consequently it may be advantageous to use them instead of argon. However, the cost of argon over plant lifetime turns out to be only 1/10 to 1/3 of the first year variable costs (FYVC), depending on the size of the storage system.

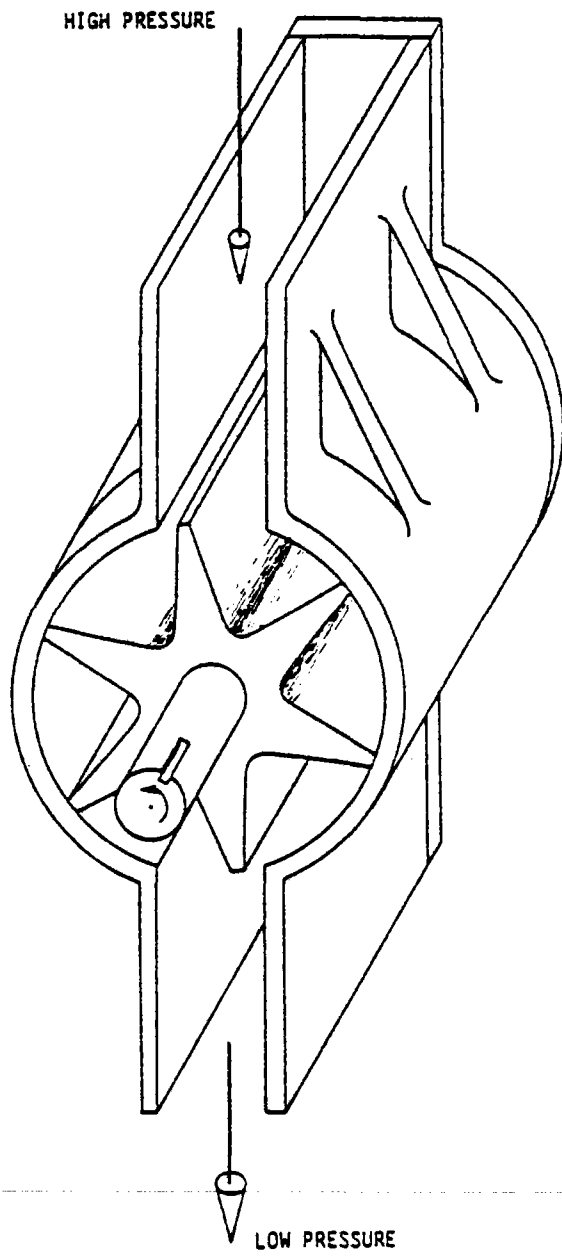


Fig. F-1 Rotary valve depressurizer.

APPENDIX G

RADIATIVE HEATING OF SLAG BEADS IN SOLAR RECEIVER

The configuration and absorbing medium of the solar receiver poses a unique problem in radiative transfer whose solution is essential to the application of the concepts outlined in this report to solar energy power systems. The essential requirement for the receiver is that the solar radiation be efficiently coupled to the beads and that radiation losses be minimal.

Because the slags considered for the absorbing and storage medium are generally transparent (when pure) over a sizable portion of the solar spectrum, heating the beads effectively will require doping the slag with an efficient absorber of solar radiation. Suitable dopants might be oxides of iron or chromium, or carbon particles. Various impurities which are likely to contaminate the slag in the other components of the power system may render the slag relatively opaque. Our own experience with RF induction melting of small samples of slag supports this. Usually after two to three successive melts the slags take on a dark gray, opaque color as a result of contamination by impurities leached from the crucible and other components in contact with the slags.

A complete analysis of the heating of the beads must include absorption and scattering by the beads of both direct and reradiated solar flux, emission by the beads, absorption and reradiation by the sidewalls of the cavity and convective losses to the air in the cavity. We are presently formulating a four-flux model of the radiative transport phenomena which occur in the droplet heat exchanger, whose geometry and operation bear a strong resemblance to the proposed solar cavity. This work is not yet

complete, however, a rough estimate of the heating of the beads has been obtained from a simple radiative model which assumes that the cloud of beads is optically thin and that scattering from the beads can be neglected.

The model assumes that the vertical cylindrical sidewall of the cavity (see Fig. 9, Section 3.10) is at the equilibrium blackbody temperature corresponding to the solar flux density impinging on it. The top end of the cavity is assumed to be at the inlet bead temperature and the bottom end (the surface of the molten pool of slag) is at the slag exit temperature. The solar flux is assumed to enter the cavity horizontally. Viewed from above, the solar flux from the heliostat field converges to a focal plane coincident with the aperture of the receiver and thence diverges to fill the cavity. The aperture is arbitrarily assumed to have a width of 1.4 times the cavity radius and a height equal to the active height of the cavity. It is assumed that the solar flux which fills the cavity is uniform over the diameter and height of the cavity.

The slag beads are injected at their terminal velocity and are assumed to interact radiatively with the solar flux and with the walls of the cavity, but not with each other. Convective heat loss from the beads to the ambient air and the heat of fusion of the beads are neglected. Writing the heat balance for a falling bead under these assumptions we obtain:

$$\frac{dT_p}{dx} = \frac{3\epsilon I}{2C_s \rho_p U_p d} + \frac{6\epsilon\sigma}{C_s \rho_p U_p d} [F_{12}(T_2^4 - T_p^4) + F_{13}(T_3^4 - T_p^4) + F_{14}(T_4^4 - T_p^4) - F_{15}(T_p^4 - T_5^4)]$$

where T_p , ρ_p , U_p , C_s and d are respectively the temperature, density, terminal velocity, specific heat and diameter of the bead; ϵ is the

emissivity of the bead, I is the incident solar flux density and σ is the Stefan-Boltzmann radiation constant. T_2 , T_3 and T_4 are, respectively, the temperatures of the cylindrical wall, top and bottom, of the receiver cavity. T_5 is the ambient temperature outside the receiver. The F_{ij} 's are the geometrical radiation configuration factors¹ between the bead and the respective surfaces of the cavity. F_{15} is the configuration factor between the bead and the cavity aperture; accordingly the last term in the equation represents the reradiation loss from the bead through the aperture to the external surroundings. Analytical expressions for the F_{ij} 's as functions of bead position were obtained from literature sources² for a bead traveling along the centerline of the cavity. The configuration factors of off-axis beads vary by no more than 30% from the axial values.²

The above equation was numerically integrated for beads of 1 mm dia ($\rho_p = 2.9 \text{ g/cm}^3$, $C_s = 0.3 \text{ cal/gm}^\circ\text{K}$) falling at terminal velocity in 800°K air and having an emissivity of 0.5. The beads were assumed to enter the cavity at 900°K and to exit at 1700°K .^{*} The external ambient temperature was assumed to be 300°K . A uniform average solar flux of 1 MW/m^2 (equivalent to a concentration ratio of 1000) inside the cavity was assumed.

Under these conditions the beads have a terminal velocity of 9.22 m/sec and the cylindrical sidewall attains an equilibrium temperature of 2050°K . A receiver 3 m diameter \times 12 m high heats the beads to the desired temperature of 1700°K , as shown in Fig. G-1. Also shown are the results obtained assuming an intracavity average solar flux density of 2 MW/m^2 . In this case the cavity has a height of $\sim 6 \text{ m}$. If the beads are admitted at

^{*}Normally, the beads would enter at 980°K and the molten slag would exit at 1650°K . The wider temperature range used in the present example corresponds to system startup conditions.

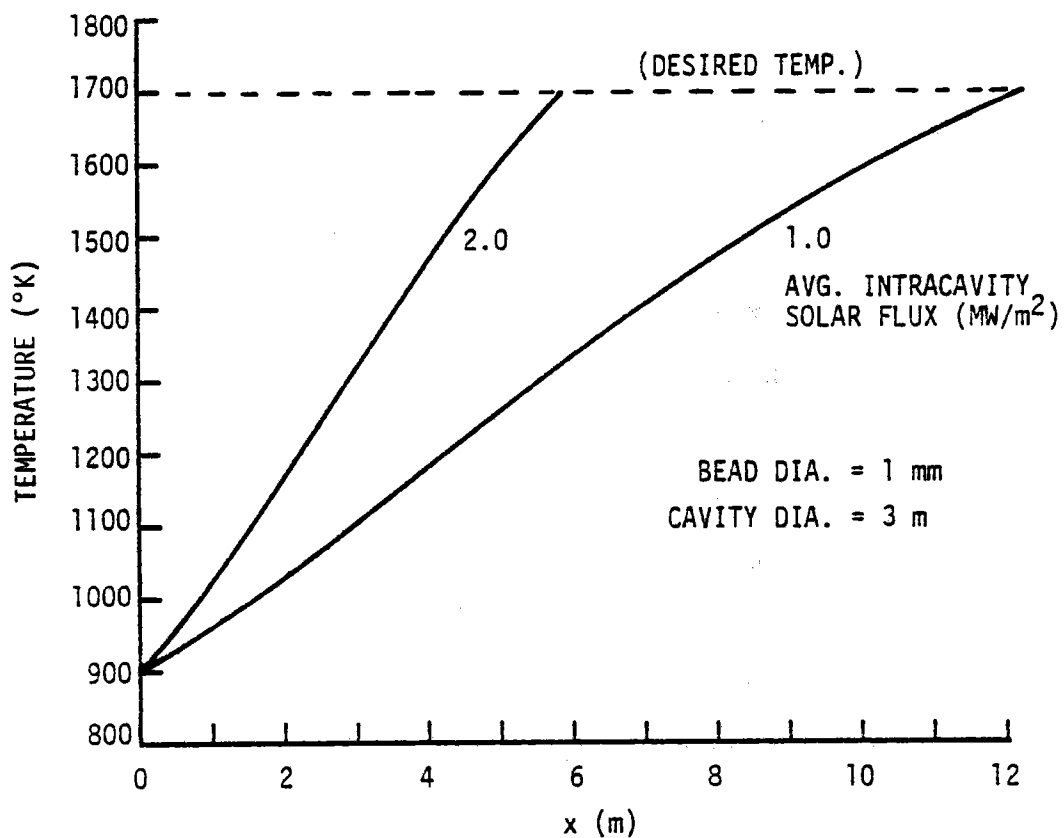


Fig. G-1 Axial temperature profiles of slag beads falling at terminal velocity through vertical cylindrical solar receiver cavity for various solar fluxes. (x denotes distance from top of cavity. Air temperature assumed to be 800°K.)

300°K ambient temperature, they are heated to only ~1270°K, hence, for a dead cold start, preheating of the beads to 900°K is necessary.

The efficiency η_c of the receiver configuration is given by:³

$$\eta_c = 1 - \frac{\sigma T_c^4}{I_a} \left(\frac{A_a}{A_c} \right)^2$$

where T_c is the cavity wall temperature, I_a is the solar flux density at the cavity aperture, A_a is the aperture area and A_c is the cavity frontal area. For the case of 1 MW/m² average internal flux, $I_a = 1.4$ MW/m² for an aperture 1.4 times the cavity radius. Assuming $T_c = T_2$ (a conservative assumption since T_3 and T_4 are both less than T_2) we obtain $\eta_c \approx 65\%$.

Based on the assumptions made in this model, the above results should only be considered to be approximate. In particular, the inclusion of interparticle radiative interactions will modify the results. The importance of these interactions can be estimated from a calculation of the radiation mean free path in the cavity.

The required mass flow of beads is 1.0×10^5 kg/hr. Assuming that the beads are uniformly distributed, this results in a bead volume fraction, β (i.e., the fraction of cavity volume occupied by beads) of 1.5×10^{-4} . If we take the total scattering and absorption cross section to be equal to three times the geometrical cross-section of the beads, then the mean free path of radiation in the cavity is given by $\lambda_\sigma = 2d/9\beta$ (see Appendix C). In the present case we obtain $\lambda_\sigma \approx 1.5$ m which is half the diameter of the cavity. Thus, interparticle radiative interactions are important both in the radial and axial directions and must be included in a more comprehensive model. It follows that the reradiation from the cavity walls and the beads themselves

will be trapped within the cloud of falling beads and thus reradiation losses will be significantly lower than if the cloud were optically thin. Consequently, the receiver efficiency will actually be higher than the 65% calculated above.

The model discussed here is admittedly oversimplified and provides only approximate results, but it does serve to indicate that it should be possible to heat slag beads to the desired temperature range using a reasonably sized solar receiver cavity and attainable concentration ratios.

References - Appendix G

1. R. Siegel and J.R. Howell, Thermal Radiation Heat Transfer, 2nd ed., McGraw Hill, New York, 1981.
2. A. Feingold and K.G. Gupta, "New Analytical Approach to the Evaluation of Configuration Factors in Radiation from Spheres and Infinitely Long Cylinders," J. Heat Transfer 92, 72, 1970.
3. P.O. Jarvinen, "Windowed Versus Windowless Solar Energy Cavity Receivers," Proc. 11th Intersociety Energy Conversion Engineering Conference, 1244, 1976.

| | | | |
|--|---|---|------------------------------|
| Document Control Page | 1. SERI Report No. SERI/STR-231-1812 | 2. NTIS Accession No. | 3. Recipient's Accession No. |
| 4. Title and Subtitle High Temperature Integrated Thermal Energy Storage for Solar Thermal Applications | | 5. Publication Date November 1982 | |
| 7. Author(s) A. P. Bruckner, A. Hertzberg | | 8. Performing Organization Rept. No. | |
| 9. Performing Organization Name and Address Aerospace and Energetics Research Program University of Washington Seattle, WA 98195 | | 10. Project/Task/Work Unit No. 1298.11 | |
| | | 11. Contract (C) or Grant (G) No. (C) XP-9-9371-1 (G) | |
| 12. Sponsoring Organization Name and Address Solar Energy Research Institute 1617 Cole Boulevard Golden, Colorado 80401 | | 13. Type of Report & Period Covered Technical Report | |
| 15. Supplementary Notes Technical Monitor: Werner Luft | | 14. | |
| 16. Abstract (Limit: 200 words) This report presents an analysis of a novel, very high temperature solar thermal energy storage system which uses molten slag as the storage medium. Slag bead aggregate is melted in a solar central receiver and stored in liquid form at 1650 K in an insulated refractory storage vessel. Sensible heat is extracted from the molten slag in a direct-contact droplet heat exchanger, in which the slag is sprayed as a multitude of droplets through a high pressure counter-flowing working gas. The heated gas is used in a high-temperature regenerative Brayton cycle. The solidified slag droplets are returned to the solar receiver to repeat the cycle. Capital cost and present worth revenue requirement data are developed from a 10 MW _e point-design electric power system for 1, 6, 15 and 48 hour storage. | | | |
| 17. Document Analysis a. Descriptors Brayton cycle power systems ; Central receivers ; Cost ; Design ; Direct contact heat exchangers ; Economic analysis ; Feasibility studies ; Latent heat storage ; Present worth method ; Refractories ; Slags ; Solar thermal power plants ; Tanks ; Thermodynamic properties ; Very high temperature Identifiers/Open-Ended terms Conceptual design c. UC Categories 62 | | | |
| 18. Availability Statement National Technical Information Center U.S. Department of Commerce 5285 Port Royal Road Springfield, Virginia 22161 | | 19. No. of Pages 116 | |
| | | 20. Price \$6.50 | |